Contents

1 Models and Discretization

In this chapter, the mathematical description of the multi-scale model and its discretization is presented. We use the multi-scale chemo-electro-mechanical model that was introduced in the literature [Röh12]; [Hei13]; [Hei15]; [Mor15]. Additional models known from literature are incorporated that were previously only simulated in isolation: The multidomain description for electrophysiology [Klo20], a model of neural stimulation [Cis08] and a sensory organ models such as muscle spindles [Mil06b]. Similarly, models of Golgi tendon organs can be added [Mil06a].

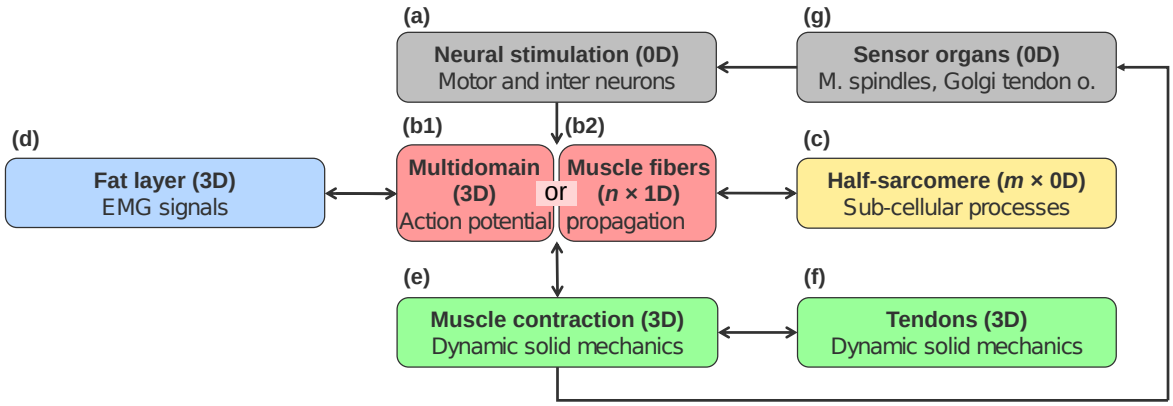

Figure 1.1: Interacting components of the multi-scale model.

Figure 1.1 shows an overview of the components of the implemented multi-scale model. A pool of motor neurons drives the stimulation of the muscular system in Fig. 1.1 (a). The axons of each motor neuron innervate the muscle fibers corresponding to the same MU and transmit rate-encoded stimulation signals.

In the muscle tissue, action potentials propagate starting at the neuromuscular junctions and subsequently reaching the whole length of the muscle. In our multi-scale model, two different formulations are available to describe this phenomenon. The multidomain description (Fig. 1.1 (b1)) models the MUs from a homogenized 3D perspective. The description with muscle fibers (Fig. 1.1 (b2)) models action potential propagation explicitely with n 1D muscle fibers.

Both of these descriptions of electrophysiology involve a subcellular model (Fig. 1.1 (c)). This model describes the ionic processes involving the fiber membranes and taking place within one half of a sarcomere as the smallest unit to generate muscle forces. A large number m of instances of this model have to be computed.

In addition to the physiology of the muscle, a layer of body fat and skin can be added on top of the muscle belly. This 3D fat layer (Fig. 1.1 (d)) is used to simulated EMG recordings on the skin surface. The model for the fat layer is unidirectionally coupled with the muscle fiber model (Fig. 1.1 (b2)) or bidirectionally coupled with the multidomain model (Fig. 1.1 (b1)). Using the multidomain model, it is, thus, possible to simulate external stimulation by electrodes on the skin which is subject to research in neuroprosthetics.

An activated muscle generates force. On the cellular level, this can be computed by the half-sarcomere model (c). On the macroscopic scale, stresses lead to strains and contraction of the muscle. This is described by the muscle contraction model on a 3D domain (Fig. 1.1 (e)). This description is coupled with the electrophysiology models (b1),(b2) by the geometry of the contracting muscle and fibers and with the subcellular model by the generated active stresses of the half-sarcomere. Displacements and stresses can be computed for the muscle belly itself, but also for the connected body fat layer and for elastic tendons (Fig. 1.1 (f)). Depending on the research questions, the contraction model is either formulated quasi-static or fully dynamic, taking into account inertia effects.

Sensory organs such as muscle spindles and Golgi tendon organs sense fiber stretch and contraction velocity (Fig. 1.1 (g)). They are connected with the motor neuron pool by layers of interneurons and modulate the stimulation in Fig. 1.1 (a).

1.1 Model equations

1.1.1 Subcellular model

Propagation of electric stimuli along muscle fibers involves activation and deactivation of ion channels and ion pumps in the fiber membrane, the sarcolemma and in the transverse tubules. Functioning of these processes on the subcellular scale have first been suggested in 1952 by Hodgkin and Huxley after their studies of the squid giant axons [Hod52a]; [Hod52b]. To date, their mathematical model still serves as the basis for electrophysiology models and some of their predictions, e.g. on gating currents that occur during opening of channels, were experimentally confirmed later.

The fiber membrane separates intra and extracellular space and can be locally described by an electric circuit. The membrane voltage $V_m = \phi_i - \phi_e$ is the difference between the intra and extracellular potentials, ϕ_i and ϕ_e. The membrane stores charges Q, quantifiable by its electric capacitance C_m:

$$Q = C_m \cdot V_m. \tag{1.1}$$

A change in transmembrane potential, e.g., induced by an action potential leads to a change of Q, which subsequently is accounted for by an electric current I over the membrane. This can be formally obtained by deriving Eq. (1.1) with respect to time:

$$\frac{\mathrm{d}Q}{\mathrm{d}t} = C_m \cdot \frac{\mathrm{d}V_m}{\mathrm{d}t}. \tag{1.2}$$

The current $I = \mathrm{d}Q/\mathrm{d}t$ is realized by ion passing through the membrane. Significant ions in this process are sodium (Na^+) and potassium ions (K^+). Considering a particular point of the fiber, these ions diffuse through ion-specific channels in the membrane. The diffusion is driven by an interplay of the ion concentration gradient and the electric field that is caused by an action potentials.

Without any electric field imposed by action potentials, the equilibrium state of the diffusion process for sodium and potassium ions is given by the Nernst potentials E_{Na^+} and E_{K^+}. These voltage levels depend on logarithmic relations between extra- and intracellular concentrations scaled by constants describing the thermic energy and number of electrons. In thermodynamic equilibrium, the membrane voltage is equal to the Nernst potential E_i of the involved ions i. At a higher membrane voltage V_m, the remainder $(V_m - E_i)$ is the part of the electric field that drives the ion fluxes and electric currents through the membrane. The currents depends on the conductivity g_i of the membrane for ion i.

Apart from sodium and potassium ions, the diffusion of less frequent ions and ionic pumps can be lumped by a leakage current I_L that is modelled by a channel with constant conductivity $\bar{g}_L$. Then, the total ionic membrane current I_{ion} is formulated as

$$I_{\mathrm{ion}}(V_m) = I_{Na^+} + I_{K^+} + I_L \tag{1.3a}$$

$$= g_{Na^+}(V_m - E_{Na^+}) + g_{K^+}(V_m - E_{K^+}) + \bar{g}_L(V_m - E_L). \tag{1.3b}$$

The conductivities for the sodium and potassium channels, g_{Na^+} and g_{K^+}, depend on the transmembrane voltage V_m and its history. In addition to the ionic current I_{ion}, an externally driven current I_{ext} can be modelled that occurs as a result of neural stimulation at the neuromuscular junctions. Substituting the current $I = \mathrm{d}Q/\mathrm{d}t$ in Eq. (1.2), we get

the following differential equation for the membrane voltage V_m:

$$C_m \cdot \frac{\mathrm{d}V_m}{\mathrm{d}t} = -I_{\text{ion}}(V_m) + \frac{I_{\text{ext}}}{A}. \tag{1.4}$$

The negative sign of the ionic current I_{ion} is in accordance with the definition of the membrane voltage as $V_m = \phi_i - \phi_e$. The external current I_{ext} is divided by the surface area A of the stimulating electrode or neuromuscular junction, as the description considers an infintesimal membrane area.

Hodgkin and Huxley suggested that ion channels can activate and deactivate. This process on a molecular scale requires independent "gating" particles to move to a new position in order for the channels to activate. For the potassium channel, four of these independent events have to occur, modelled by a propability n. For the sodium channel, three such particles are assumed for activation and one for deactivation of the channel, described by the gating variables m and h, respectively. The values of the gating variables change over time and modulate the conductivities of the ion channels:

$$g_{\text{Na}^+} = \bar{g}_{\text{Na}^+} \cdot m(t)^3 \cdot h(t), \qquad g_{\text{K}^+} = \bar{g}_{\text{K}^+} \cdot n(t)^4,$$

where $\bar{g}_{\text{Na}^+}$ and $\bar{g}_{\text{K}^+}$ are channel specific constants. The gating variables n, m and h can be interpreted as probabilities for the events to occur or as the amount of occured events related to all possibilities. The transition between the active state n and the non-active state $(n-1)$ is modeled by the following ordinary differential equation (ODE):

$$\frac{\mathrm{d}n}{\mathrm{d}t} = \alpha_n(V_m) \cdot (1-n) + \beta_n(V_m) \cdot n,$$

analogously for h and n. The transition rates α_n and β_n between the two states are nonlinearly dependent on the membrane voltage V_m.

For a constant V_m, this ODE has an analytical solution

$$n(t) = n_\infty\big(1 - \exp(1 - \frac{1}{\tau_n}\, t)\big), \tag{1.5}$$

which for $t \to \infty$ converges to the equilibrium value $n_\infty := \alpha\tau_n$ as shown in Fig. 1.2. The time constant $\tau_n := 1/(\alpha_n + \beta_n)$ indicates how fast the solution approaches the equilibrium, e.g., when starting from $n(0) = 0$, half of the value of the equilibrium is reached after $t_{1/2} = \log(2)\,\tau_n$. The smaller τ_n is, the stiffer is the ODE, which needs to be considered in the choice of a suitable numerical solution scheme.

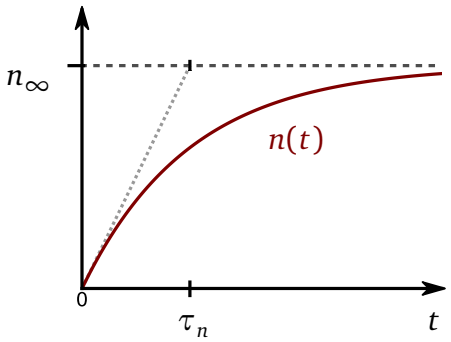

Figure 1.2: Subcellular model: Graph of the analytic solution (red) of the ordinary differential equation that is part of the activation model of ion channels for constant transmembrane voltage and initial condition $n(0) = 0$, given in Eq. (1.5). The variables n_∞ and τ_n can be interpreted as the equilibrium value and the time constant, respectively.

Because the transmembrane voltage V_m changes over time, the ODEs for n, m and h have to be solved numerically. Then, the ionic current I_{ion} is computed from the states, yielding a system of differential-algebraic equations (DAE).

The internal states in this model can be summarized by a state vector $\mathbf{y} = (n, m, h)^\top$. The combined right hand side for all states is formulated as a vector-valued function $G(V_m, \mathbf{y})$. In summary, the system of DAEs for the subcellular model can be written in the following form:

$$\frac{\partial \mathbf{y}}{\partial t} = G(V_m, \mathbf{y}), \qquad I_{\text{ion}} = I_{\text{ion}}(V_m, \mathbf{y}) \quad \text{on } \Omega_s. \tag{1.6}$$

For an exemplary solution that shows how the membrane potential changes over time, see **??**.

The system of equations in Eq. (1.6) together with Eq. (1.4) describes the subcellular processes on a single point $\Omega_s \subset \Omega_f$ on a muscle fiber Ω_f. It does not model the interaction between neighboring points that leads to propagation of action potentials. To account for action potential propagation, ionic currents I_{ion} on multiple points are coupled within the multidomain or fiber models that are formulated in the multi-scale framework. This is described in the next chapters. Then, the system of ODEs in Eq. (1.6) has to be solved for multiple subcellular points Ω_s^i in the muscle domain.

After this model, which was proposed by Hodgkin and Huxley in 1952, more detailed models were formulated that take into account more ion channels, ion pumps and more advanced biochemical processes within the cell. One particular model is the one proposed

by Shorten et al. [Sho07], which adds the full pathway from activation to excitation-contraction coupling in the sarcomere. It has a state vector of $\mathbf{y} \in \mathbb{R}^{56}$ and is used to compute active stresses for simulations of muscle contraction. Apart from I_{ion}, another value $\gamma = H(\mathbf{y}, \dot{\lambda}_f)$ is computed from the vector of states $\mathbf{y}$ and the fiber contraction velocity $\dot{\lambda}_f$, which is given to the model as a parameter. The value γ is a lumped activation parameter in the range $\gamma \in [0, 1]$ that can be linked to the continuum mechanics model of muscle contraction.

1.1.2 Bidomain model

A description of electrophysiology on general 3D muscle tissue is given by the bidomain model formulated by [Tun78]; [Pes79]. It models intra (index i) and extracellular space (index e) in a homogenized setting, such that the two domains coexist at every spatial point $\mathbf{x} \in \Omega \subset \mathbb{R}^3$. Similar to the setting of the subcellular model, the two domains in the bidomain model have locally varying electric potential fields ϕ_i and ϕ_e that yield a locally varying transmembrane voltage $V_m = \phi_i - \phi_e$. Electric conduction within the two domains is governed by conductivity tensors $\boldsymbol{\sigma}_i$ and $\boldsymbol{\sigma}_e$. Assuming static conditions, a spatially varying electric potential ϕ induces the electric field $E = -\operatorname{grad} \phi$. According to Ohm's law, the resulting current density j is given by

$$j = \boldsymbol{\sigma} E = -\boldsymbol{\sigma} \operatorname{grad} \phi \quad \text{in } \Omega. \tag{1.7}$$

This holds for both domains, yielding expressions for j_i and j_e. Intra and extracellular domain are electrochemically coupled. Thus, one assumption is that charges are preserved and a change in current density on one domain corresponds to the opposite change in current density in the other domain. This is expressed by the divergence of the current densities, which in one domain equals to the negated value in the other domain:

$$\operatorname{div}(j_i) = -\operatorname{div}(j_e) \quad \text{in } \Omega. \tag{1.8}$$

This change in current density directly corresponds to a current flow over the membrane:

$$\operatorname{div}(j_i) = A_m I_m \quad \text{in } \Omega.$$

Here, the factor A_m describes the membrane area to domain volume relationship. It is needed to convert the units between current per volume and current per area. The mem-

brane current I_m is given by the subcellular model of Hodgkin and Huxley in Eq. (1.4). Neglecting the external current I_{ext} in Eq. (1.4) and using the formulation of the intracellular current density j_i in Eq. (1.7), we get:

$$\operatorname{div}\left(\boldsymbol{\sigma}_i \operatorname{grad}(\phi_i)\right) = A_m\left(C_m \frac{\partial V_m}{\partial t} + I_{\text{ion}}(V_m)\right) \quad \text{in } \Omega.$$

The ionic current I_{ion} can be computed by Eq. (1.3b). By plugging Eq. (1.7) also into Eq. (1.8) and rewriting the equations in terms of the extracellular potential ϕ_e and the transmembrane voltage $V_m = \phi_i - \phi_e$, we get the bidomain equations:

$$\operatorname{div}\left((\boldsymbol{\sigma}_i + \boldsymbol{\sigma}_e)\operatorname{grad}(\phi_e)\right) + \operatorname{div}\left(\boldsymbol{\sigma}_i \operatorname{grad}(V_m)\right) = 0, \tag{1.9a}$$

$$\operatorname{div}\left(\boldsymbol{\sigma}_i \operatorname{grad}(V_m)\right) + \operatorname{div}\left(\boldsymbol{\sigma}_i \operatorname{grad}(\phi_e)\right) = A_m\left(C_m \frac{\partial V_m}{\partial t} + I_{\text{ion}}(V_m)\right). \tag{1.9b}$$

With appropriate boundary conditions, these equations are often used to model cardiac electrophysiology. They also serve as basis for the fiber models in our multi-scale setting.

1.1.3 Monodomain model

One approach to modeling skeletal muscle electrophysiology is to explicitly resolve muscle fibers and compute propagating action potentials on these fibers domains. This can be done using the monodomain equation, which is a specialization of the bidomain equations for a one-dimensional intracellular space.

We assume a muscle domain $\Omega_M \subset \mathbb{R}^3$ with a number of embedded 1D manifolds $\Omega_f^j \subset \mathbb{R}^3$ for $j = 1, \ldots, n$ that represent muscle fibers. The domain Ω_M represents the extracellular space and each fiber domain Ω_f^j represents the intracellular space. It is further assumed that electric conduction in the extracellular space is directed equally to the embedded fibers. This can be stated as

$$\boldsymbol{\sigma}_i = k \cdot \boldsymbol{\sigma}_e. \tag{1.10}$$

The intracellular conductivity tensor $\boldsymbol{\sigma}_i$ (here prolonged from the scalar value σ_i on a fiber with tangent $\mathbf{a} \in \mathbb{R}^3$ to the 3D domain by $\boldsymbol{\sigma}_i = \sigma_i \mathbf{a} \otimes \mathbf{a}$) and the extracellular conductivity $\boldsymbol{\sigma}_e$ are multiples of each other with a scaling factor $k \in \mathbb{R}$.

Plugging Eq. (1.10) into the first bidomain equation, Eq. (1.9a), and restricting the

domain to a 1D fiber Ω_f^j allows to combine the terms related to ϕ_e:

$$\operatorname{div}\big(\sigma_i \operatorname{grad}(\phi_e)\big) = -\frac{k}{k+1} \operatorname{div}\big(\sigma_i \operatorname{grad}(V_m)\big).$$

Using the second bidomain equation, Eq. (1.9b), we get the expression

$$\operatorname{div}\big(\sigma_{\text{eff}} \operatorname{grad}(V_m)\big) = A_m\big(C_m \frac{\partial V_m}{\partial t} + I_{\text{ion}}(V_m, \mathbf{y})\big) \quad \text{on } \Omega_f^j.$$

The effective conductivity σ_{eff} combines the intra and extracellular conductivities, σ_i and σ_e, analogously to a parallel circuit by

$$\sigma_{\text{eff}} := \sigma_i \parallel \sigma_e = \frac{\sigma_i \sigma_e}{\sigma_i + \sigma_e}.$$

Rearranging the terms yields the classical form of the monodomain equation:

$$\frac{\partial V_m}{\partial t} = \frac{1}{A_m C_m}\big(\sigma_{\text{eff}} \frac{\partial^2 V_m}{\partial x^2} - A_m I_{\text{ion}}(V_m, \mathbf{y})\big) \qquad \text{for } x \in \Omega_f^j. \tag{1.11}$$

The multi-scale framework uses multiple instances of the monodomain equation, Eq. (1.11), together with the first bidomain equation, Eq. (1.9a), to model electrophysiology in the fibers and the extracellular domain [Mor15]. In addition to the fibers domains Ω_f^j, two instances of the muscle domain Ω_M are needed for the bidomain equation, one for the intra and one for the extracellular space. The transmembrane potential V_m is unidirectionally coupled from the fiber meshes to the intracellular space of the first bidomain equation. The extracellular potential ϕ_e corresponds to the signals that are measured during intramuscular EMG recording.

Within the multi-scale framework, it is also possible to couple a model for electric conduction in an additional layer of adipose tissue. This is described later in **??**. If no such additions should be made to the model, the following boundary conditions are prescribed:

$$\frac{\partial V_m}{\partial x} = 0 \qquad \text{on } \partial\Omega_f^j, \tag{1.12a}$$

$$\big(\boldsymbol{\sigma}_i \operatorname{grad}(V_m)\big) \cdot \mathbf{n}_m = -\big(\boldsymbol{\sigma}_i \operatorname{grad}(\phi_e)\big) \cdot \mathbf{n}_m \qquad \text{on } \partial\Omega_M, \tag{1.12b}$$

$$\big(\boldsymbol{\sigma}_e \operatorname{grad}(\phi_e)\big) \cdot \mathbf{n}_m = 0 \qquad \text{on } \partial\Omega_M, \tag{1.12c}$$

with the outward normal vector $\mathbf{n}_m$. Equation (1.12a) defines homogeneous Neumann

boundary conditions at the two ends of each 1D muscle fiber domain. Equation (1.12b) is equivalent to a homogeneous Neumann boundary condition on the intracellular current density j_i (cf. Eq. (1.7)) and is expressed in terms of the transmembrane voltage V_m and the extracellular potential ϕ_e. Another homogeneous Neumann boundary condition on ϕ_e is required in Eq. (1.12c).

1.1.4 Multidomain model

The multidomain model is an alternative approach to the description based on monodomain and bidomain equations described in Sections 1.1.2 and 1.1.3. It was formulated in [Klo20] and describes the same physics. However, the muscle fibers are homogenized and all equations are formulated using a single 3D muscle domain Ω_M.

The multidomain equations generalize the two bidomain equations and allow to take into account multiple MUs by defining a separate intracellular space for each MU. Thus, at every spatial point $\mathbf{x} \in \Omega_M$ one extracellular and N_{MU} intracellular domains or compartments coexist, where N_{MU} is the number of MUs. As before, the extracellular domain has the electric potential ϕ_e and conductivity tensor $\boldsymbol{\sigma}_e$. For each compartment $k = 1, \ldots, N_{\mathrm{MU}}$, a separate electric potential ϕ_i^k, transmembrane voltage $V_m^k = \phi_i^k - \phi_e$, conductivity tensor $\boldsymbol{\sigma}_i^k$, surface to volume ratio of the membrane A_m^k and membrane capacitance C_m^k are defined.

Analogous to the fibers of a MU that exhibit different densities at different locations in the muscle, each compartment occupies different locations within the domain to a different extent. This is described by the relative occupancy factor $f_r^k : \Omega_M \to [0,1]$ for MU k. The factors have different values in the domain according to the presence of the MU at the respective location. At every point, their sum is one, $\sum_{k=1}^{N_{\mathrm{MU}}} f_r^k = 1$, if all MUs should be considered or less than one if the effect of remainder MUs that will not be activated in the simulation scenario are neglected.

The first multidomain equation is similar to the first bidomain equation, Eq. (1.9a), and balances the current flow between the extracellular space and the weighted sum of all intracellular spaces:

$$\operatorname{div}\left(\boldsymbol{\sigma}_e \operatorname{grad}(\phi_e)\right) + \sum_{k=1}^{N_{\mathrm{MU}}} f_r^k \operatorname{div}\left(\boldsymbol{\sigma}_i^k \operatorname{grad}(V_m^k + \phi_e)\right) = 0. \tag{1.13}$$

By defining a total intracellular conductivity tensor $\boldsymbol{\sigma}_i = \sum_{k=1}^{N_{\mathrm{MU}}} f_r^k \boldsymbol{\sigma}_i^k$, Eq. (1.13) can be restated as

$$\operatorname{div}\big((\boldsymbol{\sigma}_e + \boldsymbol{\sigma}_i)\operatorname{grad}(\phi_e)\big) + \sum_{k=1}^{N_{\mathrm{MU}}} f_r^k \operatorname{div}\big(\boldsymbol{\sigma}_i^k \operatorname{grad}(V_m^k)\big) = 0. \tag{1.14}$$

The second multidomain equation equals the second bidomain equation, Eq. (1.9b). It describes the current over the membrane and holds for every compartment:

$$\operatorname{div}(\boldsymbol{\sigma}_i^k \operatorname{grad}(V_m^k + \phi_e)) = A_m^k \left(C_m^k \frac{\partial V_m^k}{\partial t} + I_{\mathrm{ion}}(V_m^k) \right) \qquad \forall k \in \{1, \ldots, N_{\mathrm{MU}}\}.$$

It is convenient to rearrange it for $\partial V_m^k / \partial t$:

$$\frac{\partial V_m^k}{\partial t} = \frac{1}{A_m^k C_m^k} \left(\operatorname{div}\big(\boldsymbol{\sigma}_i^k \operatorname{grad}(V_m^k + \phi_e)\big) - A_m^k I_{\mathrm{ion}}(V_m^k) \right) \quad \forall k \in \{1, \ldots, N_{\mathrm{MU}}\}. \tag{1.15}$$

The current I_{ion} over the membrane is again computed by the subcellular model given by Eq. (1.3b).

The resulting system of Equations (1.14) and (1.15) constitutes the first and second multidomain equations and can be used to compute muscle electrophysiology. The boundary conditions are defined analogous to Equations (1.12b) and (1.12c):

$$\big(\boldsymbol{\sigma}_i^k \operatorname{grad}(V_m^k)\big) \cdot \mathbf{n}_m = -\big(\boldsymbol{\sigma}_i^k \operatorname{grad}(\phi_e)\big) \cdot \mathbf{n}_m \qquad \text{on } \partial\Omega_M \qquad \forall k \in \{1, \ldots, N_{\mathrm{MU}}\}, \tag{1.16a}$$

$$\big(\boldsymbol{\sigma}_e \operatorname{grad}(\phi_e)\big) \cdot \mathbf{n}_m = 0, \qquad \text{on } \partial\Omega_M \tag{1.16b}$$

where $\mathbf{n}_m$ is the outward normal vector on $\partial\Omega_M$.

1.1.5 Electric Conduction in the Body Domain

Surface EMG signals are the result of electric conduction in the electrically active muscle tissue as well as in surrounding inactive tissue such as adipose tissue and skin or connective tissue such as tendons and ligaments. This surrounding tissue is summarized by the body domain Ω_B, which partly shares its boundary with the muscle domain Ω_M.

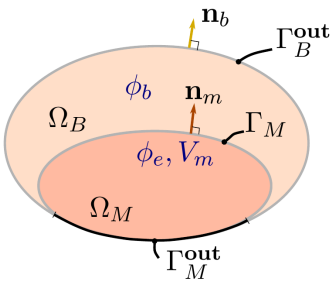

Figure 1.3: Computational domains for simulations of surface EMG. The body domain Ω_B and the muscle domain Ω_M share a part of their boundary, Γ_M, which has a normal vector $\mathbf{n}_m$. The outer boundary is composed of Γ_B^{out} and Γ_M^{out} and has the outward normal vector $\mathbf{n}_b$.

Figure 1.3 visualizes these domains and defines their names: The domains Ω_M and Ω_B have outward normals $\mathbf{n}_m$ and $\mathbf{n}_b$, the outer boundary is composed of Γ_B^{out} and Γ_M^{out} and the variables ϕ_e, V_m and ϕ_b are defined within the respective domains.

The work of [Mor15] proposes an isotropic conductivity $\boldsymbol{\sigma}_b$ and a harmonic electric potential ϕ_b in the body domain Ω_B:

$$\operatorname{div}\left(\boldsymbol{\sigma}_b \operatorname{grad}(\phi_b)\right) = 0 \qquad \text{on } \Omega_B. \tag{1.17}$$

The electric potentials ϕ_e and ϕ_b of the neighboring domains Ω_M and Ω_B as well as the current densities are continous on the shared boundary Γ_M. This is described by the following coupling conditions:

$$\phi_e = \phi_b \qquad \text{on } \Gamma_M, \tag{1.18a}$$

$$\left(\boldsymbol{\sigma}_e \operatorname{grad}(\phi_e)\right) \cdot \mathbf{n}_m = \left(\boldsymbol{\sigma}_b \operatorname{grad}(\phi_b)\right) \cdot \mathbf{n}_m \qquad \text{on } \Gamma_M. \tag{1.18b}$$

On the outer boundary Γ_B^{out}, homogeneous Neumann boundary conditions are assumed:

$$\left(\boldsymbol{\sigma}_b \operatorname{grad}(\phi_b)\right) \cdot \mathbf{n}_b = 0 \qquad \text{on } \Gamma_B^{\text{out}}. \tag{1.19}$$

The description of the body domain has to be combined either with the fiber based description in Sec. 1.1.3 or the multi-domain description in Sec. 1.1.4. In the literature, this combination was mathematically described for the fiber-based model in [Mor15] and for the fiber based model in [Klo20]. Correspondingly, additional boundary conditions either in Eq. (1.12) or in Eq. (1.16) are assumed: For the fiber based description, which

uses the bidomain equation for volume conduction, the boundary conditions are:

$$\big(\boldsymbol{\sigma}_i \operatorname{grad}(V_m)\big)\cdot \mathbf{n}_m = -\big(\boldsymbol{\sigma}_i \operatorname{grad}(\phi_e)\big)\cdot \mathbf{n}_m \qquad \text{on } \partial\Omega_M = \Gamma_M \cup \Gamma_M^{\text{out}}, \tag{1.20a}$$

$$\big(\boldsymbol{\sigma}_e \operatorname{grad}(\phi_e)\big)\cdot \mathbf{n}_m = 0 \qquad \text{on } \partial\Gamma_M^{\text{out}}. \tag{1.20b}$$

For the multidomain description with fat layer, the boundary conditions are:

$$\big(\boldsymbol{\sigma}_i^k \operatorname{grad}(V_m^k)\big)\cdot \mathbf{n}_m = -\big(\boldsymbol{\sigma}_i^k \operatorname{grad}(\phi_e)\big)\cdot \mathbf{n}_m \qquad \text{on } \partial\Omega_M = \Gamma_M \cup \Gamma_M^{\text{out}}, \tag{1.21a}$$

$$\big(\boldsymbol{\sigma}_e \operatorname{grad}(\phi_e)\big)\cdot \mathbf{n}_m = 0 \qquad \text{on } \partial\Gamma_M^{\text{out}}. \tag{1.21b}$$

The first condition in Eq. (1.21a) is enforced for all compartments $k = 1, \ldots, N_{\text{MU}}$.

1.1.6 Model of Muscle Contraction

Muscle contraction is described on the organ level by a description of solid mechanics. Because of possibly large strains, a nonlinear hyperelastic formulation is used. For mathematical foundations in continuum mechanics, we refer to basic literature such as the books of Holzapfel [Hol00] and Marsden and Hughes [Mar94], as well as literature of the application of the Finite Element Method in continuum mechanics [Zie77]; [Sus87]; [Zie05].

We consider the 3D muscle domain $\Omega_0 = \Omega_M \subset \mathbb{R}^3$ in reference configuration at time $t = 0$ that deforms into a current configuration Ω_t at time t. The material points are given by $\mathbf{X} \in \Omega_0$. The corresponding points $\mathbf{x} \in \Omega_t$ in the current configuration are defined by the placement function $\mathbf{x} = \chi_t(\mathbf{X})$. In the following, capital letters refer to quantities in material or Lagrangian description, i.e., defined in the reference configuration and small letters refer to quantities in Eulerian description, i.e., defined in the current configuration.

The relation of points in the current configuration with respect to their reference configuration can also be described by the displacements field $\mathbf{u}$:

$$\mathbf{x}(\mathbf{X}) = \mathbf{X} + \mathbf{u}(\mathbf{X}).$$

The current velocity $\mathbf{v}$ is the time derivative of the displacements, $\mathbf{v} := \dot{\mathbf{u}}$.

The foundation of continuum mechanics usually assumes three balance principles: conversation of mass, momentum and angular momentum. In the following, these principles are presented in their Eulerian forms. First, we assume conservation of mass in terms of the densities in reference and current configurations, $\rho_0(\mathbf{X})$ and $\rho(\mathbf{x})$:

$$\int_{\Omega_0} \rho_0 \, \mathrm{d}V = \int_{\Omega_t} \rho \, \mathrm{d}v.$$

With the intermediate step of deducing $\mathrm{d}/\mathrm{d}t \int_{\Omega_t} \rho \, \mathrm{d}v = 0$, we get the following differential equation:

$$\dot{\rho}(\mathbf{v}, t) + \rho(\mathbf{x}, t) \operatorname{div}\big(\mathbf{v}(\mathbf{x}, t)\big) = 0. \tag{1.22}$$

As muscle tissue largely consists of water, we assume an incompressible domain. This is equivalent to a constant density and, thus, Eq. (1.22) reduces to

$$\operatorname{div}(\mathbf{v}(\mathbf{x}, t)) = 0. \tag{1.23}$$

The second assumption is the balance of momentum, which is expressed by

$$\frac{\mathrm{d}}{\mathrm{d}t} \int_{\Omega_t} \rho \, \mathbf{v} \, \mathrm{d}v = \int_{\Omega_t} \rho \, \mathbf{b} \, \mathrm{d}v + \int_{\partial\Omega_t} \mathbf{t} \, \mathrm{d}a.$$

Here, $\mathbf{b}$ describes a body force and $\mathbf{t}$ describes a traction force that acts on the surface of the current configuration. The corresponding local form is given by the following differential equation:

$$\rho \, \dot{\mathbf{v}}(\mathbf{x}, t) = \rho \, \mathbf{b}(\mathbf{x}, t) + \operatorname{div} \boldsymbol{\sigma}(\mathbf{x}, t). \tag{1.24}$$

The second order Cauchy stress tensor $\boldsymbol{\sigma}$ has units of force per area and is defined by the relation $\mathbf{t} = \boldsymbol{\sigma}\mathbf{n}$ between a traction force $\mathbf{t}$ in a virtual cut out of the body at $\mathbf{x}$ with normal vector $\mathbf{n}$.

The third assumption is the balance of angular momentum and can be formulated using the 3D cross-product:

$$\frac{\mathrm{d}}{\mathrm{d}t} \int_{\Omega_t} \mathbf{x} \times (\rho \, \mathbf{v}) \, \mathrm{d}v = \int_{\Omega_t} \mathbf{x} \times (\rho \, \mathbf{b}) \, \mathrm{d}v + \int_{\partial\Omega_t} \mathbf{x} \times \mathbf{t} \, \mathrm{d}a.$$

Derivations yield equivalence to the symmetry of the Cauchy stress tensor, $\boldsymbol{\sigma} = \boldsymbol{\sigma}^\top$.

A further assumption is to only consider isothermal conditions. An activated muscle performs work and by metabolism energy is added to the system. Further, the muscle is not thermodynamically isolated. The system is not closed regarding conversion and transfer of energy and, thus, the balance of energy cannot be modeled easily.

The mathematical description has to be closed by defining a constitutive relation between stresses and strains. This can be done by a strain energy function Ψ. It is usually formulated in terms of the five principle strain invariants I_1 to I_5. A derivative of Ψ is used to derive a term for the stress. More details are given in Sec. 1.3.

In the muscle contraction model of [Hei13], the strain energy function is additively composed of two passive terms, one isotropic and one anisotropic, and an additional term for the active stress that depends on the activation parameter γ and models the generated muscle force:

$$\Psi(I_1, I_2, I_4, I_5) = \Psi_{\text{isotropic}}(I_1, I_2) + \Psi_{\text{anisotropic}}(I_4, I_5) + \Psi_{\text{active}}(\gamma).$$

Note the missing dependency on the third invariant I_3, which is constant because of the enforced incompressiblity.

The passive behaviour of muscle tissue is modeled by a transversely isotropic Mooney-Rivlin material. The isotropic part is given by the Mooney-Rivlin formulation:

$$\Psi_{\text{isotropic}}(I_1, I_2) = c_1 (I_1 - 3) + c_2 (I_2 - 3). \tag{1.25}$$

The values of the two material parameters c_1 and c_2 can be determined by compression tests and are summarized in the work of [Hei13].

The anisotropic behaviour depends on the fiber stretch $\lambda_f = \sqrt{I_4}$. The formulation in [Hei13] uses two material parameters b and d and the following function:

$$\Psi_{\text{anisotropic}}(\lambda_f) = \frac{b}{d} (\lambda_f^d - 1) - b \log(\lambda_f).$$

The active contribution is directly formulated in terms of the second Piola-Kirchhoff stress $\mathbf{S}$, which in the incompressible case is the pull-back of the Cauchy stress $\boldsymbol{\sigma}$ used in

Eq. (1.24):

$$\mathbf{S}_{\text{active}} = \frac{1}{\lambda_f} \frac{\partial \Psi_{\text{active}}}{\partial \lambda_f} \mathbf{A} \otimes \mathbf{A} = \frac{1}{\lambda_f} \cdot S_{\text{max,active}} \cdot f_\ell(\lambda_f) \cdot \bar{\gamma}\, \mathbf{A} \otimes \mathbf{A},$$

Here, the resulting active stress tensor $\mathbf{S}_{\text{active}}$ is directed according to the material fiber direction $\mathbf{A} : \Omega_0 \to \mathbb{R}^3$, scaled by the maximum active stress parameter $S_{\text{max,active}}$, a function f_ℓ that models the force-length relation and the homogenized value $\bar{\gamma}$ in the 3D domain of the activation parameter $\gamma \in [0,1]$ that is computed by the half-sarcomere model at points in the muscle domain.

For the deforming body fat layer, the active stress contribution is disregarded. For simulating tendons, different material models can be used such as the model proposed by Carniel et al. [Car17], which describes microstructural interactions between collagen fibers and their matrix in addition to the elastic response of the fibers itself. To alter the material model, the definition of Ψ can simply be changed while all other equations remain intact. Similarly, other material models can be defined using the framework of the strain energy function.

In short summary, the following system of equations describes the continuum mechanics model of muscle contraction:

$$\operatorname{div}(\mathbf{v}) = 0, \qquad \text{(incompressibility)} \tag{1.26a}$$

$$\rho\, \dot{\mathbf{v}} = \rho\, \mathbf{b} + \operatorname{div} \boldsymbol{\sigma}, \qquad \text{(balance of momentum)} \tag{1.26b}$$

$$\boldsymbol{\sigma} = \boldsymbol{\sigma}^\top, \qquad \text{(balance of angular momentum)} \tag{1.26c}$$

$$\Psi = \Psi(I_1, I_2, I_4, I_5). \qquad \text{(material model)} \tag{1.26d}$$

Dirichlet boundary conditions for the displacements $\mathbf{u}$ and velocities $\mathbf{v}$ can fix certain parts of the muscle, e.g., at the attachment of the tendons:

$$\mathbf{u}(\mathbf{x}, t) = \hat{\mathbf{u}}(t), \qquad \mathbf{v}(\mathbf{x}, t) = \hat{\mathbf{v}}(t) \qquad \text{for } \mathbf{x} \in \partial\Omega_{\text{Dirichlet}}.$$

Initial conditions for $\mathbf{u}$ and $\mathbf{v}$ define the initial pose of the muscle tissue:

$$\mathbf{u}(\mathbf{x}, 0) = \mathbf{u}_0(\mathbf{x}), \qquad \mathbf{v}(\mathbf{x}, 0) = \mathbf{v}_0(\mathbf{x}) \qquad \text{for } \mathbf{x} \in \Omega_M.$$

Additionally, Neumann boundary conditions can be used to prescribe traction forces on the surface.

The description of the multi-scale model [Röh12]; [Hei13] assumes quasi-static conditions, which means that the velocities are set to zero, $\mathbf{v} = 0$, and inertial terms are neglected. In consequence, the incompressibility constraint in Eq. (1.26a) has to be formulated differently and the balance of momentum in Eq. (1.26b) reduces to $\rho\,\mathbf{b} + \operatorname{div}\boldsymbol{\sigma} = 0$. However, our implementation extends the model to the fully dynamic formulation given in Eq. (1.26).

1.2 Discretization

The partial and ordinary differential equations described in the last section contain spatial an temporal derivatives that have to be discretized to be numerically solved. For temporal derivatives, we use timestepping schemes, for spatial derivatives, we employ the Finite Element Method. In this section, we describe the discretization of all equations within the multi-scale model. We begin with the discretization in time.

1.2.1 Discretization of the Monodomain model

Electrophysiology models typically consists of a reaction-diffusion equation. The diffusion term describes the electric conduction in the tissue and the reaction term includes the subcellular model. In our model, the monodomain equation used in the fiber based description, Eq. (1.11), and the second multidomain equation, Eq. (1.15), are equations of this type.

This type of partial differential equation is often solved using operator splitting schemes. The canonical first order scheme is Godunov splitting [Gui03]. It was used for the solution of the chemo-electro-mechanical model in [Röh12]. In addition, we also employ the second order accurate Strang splitting scheme [Str68].

In the following, the application of these two schemes is illustrated with the monodomain equation, Eq. (1.11). The right hand sides of the diffusion and reaction terms are designated as $\mathcal{L}_1$ and $\mathcal{L}_2$:

$$\mathcal{L}_1(V_m) := \frac{1}{A_m\, C_m}\, \sigma_{\text{eff}} \frac{\partial^2 V_m}{\partial x^2}\,, \qquad \mathcal{L}_2(V_m) := -\frac{1}{C_m}\, I_{\text{ion}}(V_m, \mathbf{y}).$$

Then, the monodomain equation takes the form:

$$\frac{\partial V_m}{\partial t} = \mathcal{L}_1(V_m) + \mathcal{L}_2(V_m).$$

A timestepping scheme is constructed that starts with a given initial value $V_m^{(0)}$ and computes solution values $V_m^{(i)}$ at discrete points in time $t^{(i)} = i \cdot dt$ with a fixed timestep width dt. Godunov splitting proceeds by alternatingly solving the ODEs with right hand sides $\mathcal{L}_1$ and $\mathcal{L}_2$. In the first substep per iteration, an intermediate value V_m^* is calculated, which is used as starting point for the second substep. Each of the substeps are performed using another timestepping scheme for the ODE, e.g., the explicit Euler scheme:

$$V_m^* = V_m^{(i)} + dt\,\mathcal{L}_1(V_m^{(i)}, t^{(i)}), \tag{1.27a}$$

$$V_m^{(i+1)} = V_m^* + dt\,\mathcal{L}_2(V_m^*, t^{(i)}) \tag{1.27b}$$

Strang splitting uses a similar approach with three substeps per timestep and two intermediate values V_m^* and V_m^{**}:

$$V_m^* = V_m^{(i)} + \frac{dt}{2}\,\mathcal{L}_1(V_m^{(i)}, t^{(i)}), \tag{1.28a}$$

$$V_m^{**} = V_m^* + dt\,\mathcal{L}_2(V_m^*, t^{(i)}), \tag{1.28b}$$

$$V_m^{(i+1)} = V_m^{**} + \frac{dt}{2}\,\mathcal{L}_1(V_m^{**}, t_{(i)} + \frac{1}{2}\,dt). \tag{1.28c}$$

Figure 1.4 visualizes both splitting schemes applied to the monodomain equation. The yellow arrows correspond to the solution of the 0D subcellular model. The red arrows correspond to the solution of the 1D diffusion equation. The timestepping schemes of the substeps have timestep widths dt_{0D} and dt_{1D}, respectively. The timestep width of one splitting step is $dt_{\text{splitting}}$. Depending on how the timestep widths are chosen in relation to each other, different numbers of subcycles are used in the solution of the 0D and 1D problems.

Instead of the explicit Euler method in Equations (1.27) and (1.28), other timestepping methods can be used for the substeps. We use the following schemes, which are listed as

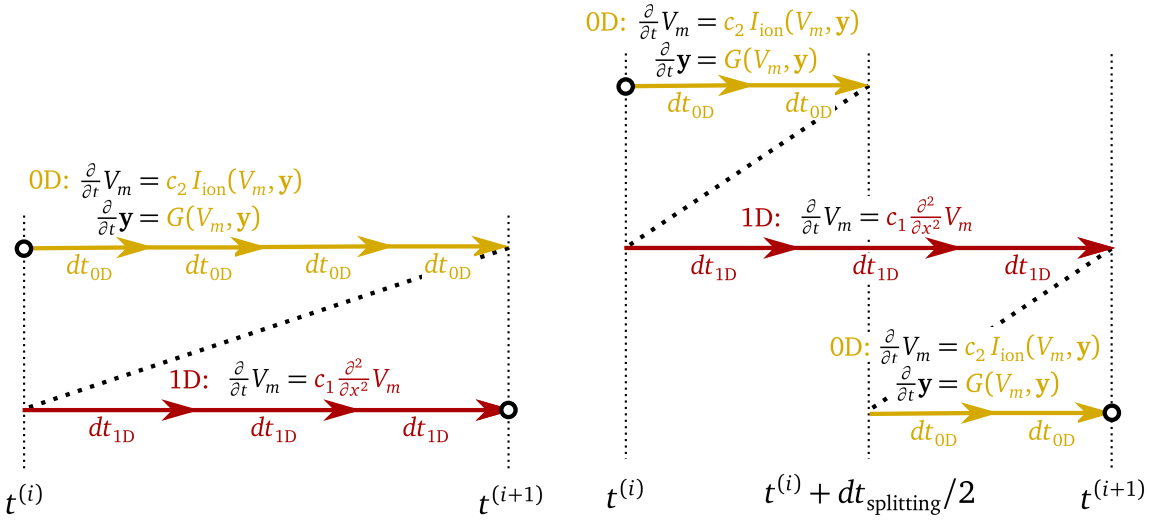

(a) The Godunov splitting uses two substeps: 0D, 1D.

(b) The Strang splitting uses three substeps: 0D, 1D, 0D.

Figure 1.4: Godunov and Strang splitting schemes that are used to solve the monodomain equation. The equation is split into a reaction part (0D,yellow) and a diffusion part (1D,red), which are solved alternatingly. The visualization shows one splitting timestep, which starts at the left circle and is completed at the right circle.

single iteration step for the generic ODE $\partial V_m/\partial t = \mathcal{L}(V_m, t)$:

$$V_m^{(i+1)} = V_m^{(i)} + dt\,\mathcal{L}(V_m^{(i)}, t^{(i)}), \tag{1.29a}$$

$$V_m^{(i+1)} = V_m^{(i)} + \frac{dt}{2}\left(\mathcal{L}(V_m^{(i)}, t^{(i)}) + \mathcal{L}\big(V_m^{(i)} + dt\,\mathcal{L}(V_m^{(i)}, t^{(i)}), t^{(i+1)}\big)\right), \tag{1.29b}$$

$$V_m^{(i+1)} = V_m^{(i)} + dt\,\mathcal{L}(V_m^{(i+1)}, t^{(i+1)}), \tag{1.29c}$$

$$V_m^{(i+1)} = V_m^{(i)} + \frac{dt}{2}\left(\theta\,\mathcal{L}(V_m^{(i+1)}, t^{(i+1)}) + (1-\theta)\,\mathcal{L}(V_m^{(i)}, t^{(i)})\right). \tag{1.29d}$$

Here, Eq. (1.29a) is the first-order accurate explicit Euler scheme, Eq. (1.29b) is the second-order accurate Heun scheme, Eq. (1.29c) is the first order accurate implicit Euler scheme and Eq. (1.29d) is the Crank-Nicolson scheme [Cra47], which for $\theta = 0$ equals the explicit Euler and for $\theta = 1$ equals the implicit Euler scheme. For $\theta = \frac{1}{2}$, it is second order accurate. An advantage of the implicit schemes in Equations (1.29c) and (1.29d) is that, for our considered diffusion problems, they are unconditionally stable. A disadvantage is that a linear equation has to be solved in every timestep.

A second order accurate timestepping scheme allows a higher timestep width to yield

the same numerical error as a first order scheme. To obtain a second order scheme for the monodomain equation, we use Strang splitting (Eq. (1.28)) with the Crank-Nicolson scheme (Eq. (1.29d)) for the diffusion term $\mathcal{L}_1$ and Heun's method (Eq. (1.29b)) for the reaction term $\mathcal{L}_2$. In the subcellular model, the system of ODEs with state vector $\mathbf{y}$ given in Eq. (1.6) is solved with Heun's method along with the equation in terms of V_m.

Next, the spatial derivatives in the diffusion part $\mathcal{L}_2$ of the split equation have to be discretized. Then, both the multidomain and the fiber based models can be solved using the splitting scheme.

1.2.2 Discretization of Diffusion and Laplace Equations

For the spatial discretization, we first derive the Finite Element formulation for a generic diffusion equation in a domain $\Omega \subset \mathbb{R}^d$ of arbitrary dimensionality d. Then, its specialization to 1D defines the formulation for the monodomain equation. Considering a 3D domain, the derived formulation is an important building block for the discretization of the multidomain model. This is shown in more detail in a later section, Sec. 1.2.4

We consider the following diffusion problem in the variable $u : \Omega \times [0, t_{\text{end}}] \to \mathbb{R}$ with Neumann boundary conditions on a part of the boundary $\Gamma_f \subset \partial\Omega$ with normal vector $\mathbf{n}$:

$$\frac{\partial u}{\partial t} = \operatorname{div}(\boldsymbol{\sigma} \operatorname{grad} u), \quad (\boldsymbol{\sigma} \operatorname{grad} u) \cdot \mathbf{n} = f \quad \text{on } \Gamma_f, \quad (\boldsymbol{\sigma} \operatorname{grad} u) \cdot \mathbf{n} = 0 \quad \text{on } \partial\Omega \backslash \Gamma_f$$

We discretize the temporal derivative using the Crank-Nicolson scheme of Eq. (1.29d). Following the procedure of the Galerkin Finite Element formulation with the Hilbert space $H_0^1(\Omega)$ of test functions ϕ that are zero on the boundary, we arrive at the following weak form:

$$\int_\Omega \left(\theta \nabla \cdot (\boldsymbol{\sigma} \nabla \mathbf{u}^{(i+1)}) + (1-\theta) \nabla \cdot (\boldsymbol{\sigma} \nabla u^{(i)})\right) \phi \, \mathrm{d}\mathbf{x} \\ = \frac{1}{dt} \int_\Omega (u^{(i+1)} - u^{(i)}) \, \phi \, \mathrm{d}\mathbf{x}, \qquad \forall \phi \in H_0^1(\Omega).$$

For brevity, we express divergence and gradient using the nabla operator. In the discretization, we choose a function space $V_h = \operatorname{span}\{\varphi_j \mid j = 1, \ldots, N\}$ to represent the solution as

$u = \sum_{j=1}^{N} u_j \phi_j$. Using divergence theorem, we obtain:

$$\begin{aligned} &\sum_{j=1}^{N} \left(\theta\, u_j^{(i+1)} + (1-\theta)\, u_j^{(i)}\right) \left(-\int_\Omega \boldsymbol{\sigma}\, \nabla\varphi_j \cdot \nabla\varphi_k \,\mathrm{d}\mathbf{x} + \int_{\partial\Omega} \left(\boldsymbol{\sigma}\, \nabla\varphi_j \cdot \mathbf{n}\right) \varphi_k \,\mathrm{d}\mathbf{x} \right) \\ &\quad = \frac{1}{dt} \sum_{j=1}^{N} \left(u_j^{(i+1)} - u_j^{(i)}\right) \int_\Omega \varphi_j\, \varphi_k \,\mathrm{d}\mathbf{x}, \qquad \forall k = 1 \ldots N. \end{aligned} \tag{1.30}$$

This iteration step can be written in matrix notation in terms of the vectors of unknowns $\mathbf{u}^{(i)} = (u_0^{(i)}, \ldots, u_N^{(i)})^\top$ at timestep i:

$$\mathbf{A}\, \mathbf{u}^{(i+1)} = \mathbf{b}(\mathbf{u}^{(i)}),$$

The system matrix $\mathbf{A}$ and the right hand side $\mathbf{b}$ are given by:

$$\mathbf{A} = \theta\, (\mathbf{K}_{\boldsymbol{\sigma}} + \mathbf{B}_{\boldsymbol{\sigma}}) - \frac{1}{dt}\, \mathbf{M}, \qquad \mathbf{b} = \left((\theta - 1)\, (\mathbf{K}_{\boldsymbol{\sigma}} + \mathbf{B}_{\boldsymbol{\sigma}}) - \frac{1}{dt}\, \mathbf{M}\right) \mathbf{u}^{(i)}.$$

The formulation uses the standard stiffness matrix $\mathbf{K}_{\boldsymbol{\sigma}}$, matrix $\mathbf{B}_{\boldsymbol{\sigma}}$ of the boundary integral and mass matrix $\mathbf{M}$, whose components are defined as

$$\mathbf{K}_{\boldsymbol{\sigma},kj} = -\int_\Omega (\boldsymbol{\sigma}\, \nabla\varphi_j) \cdot \nabla\varphi_k \,\mathrm{d}\mathbf{x}, \quad \mathbf{B}_{\boldsymbol{\sigma},kj} = \int_{\Gamma_f} \left((\boldsymbol{\sigma}\, \nabla\varphi_j) \cdot \mathbf{n}\right) \varphi_k \,\mathrm{d}\mathbf{x}, \quad \mathbf{M}_{kj} = \int_\Omega \varphi_j\, \varphi_k \,\mathrm{d}\mathbf{x}. \tag{1.31}$$

Note that after applying the divergence theorem, the definition of the stiffness matrix has a minus sign, which is correct for the positive second order derivative in the original diffusion term.

Next, we take into account the Neumann boundary condition $\boldsymbol{\sigma} \nabla u \cdot \mathbf{n} = f$ on the boundary Γ_f. The flux f over the boundary is discretized by M separate ansatz functions ψ_j on Γ_f as $f = \sum_{j=1}^{M} f_j\, \psi_j$. The flux values are summarized in a vector $\mathbf{f} = (f_1, \ldots, f_M)^\top$. Plugging this into Eq. (1.30) yields the following equation in matrix notation:

$$\tilde{\mathbf{A}}\, \mathbf{u}^{(i+1)} = \tilde{\mathbf{b}}(\mathbf{u}^{(i)}), \tag{1.32}$$

with the system matrix $\tilde{\mathbf{A}}$ and right hand side $\tilde{\mathbf{b}}$:

$$\tilde{\mathbf{A}} = \theta\, \mathbf{K}_{\boldsymbol{\sigma}} - \frac{1}{dt}\, \mathbf{M}, \qquad \tilde{\mathbf{b}} = \left((\theta - 1)\, \mathbf{K}_{\boldsymbol{\sigma}} - \frac{1}{dt}\, \mathbf{M}\right) \mathbf{u}^{(i)} - \mathbf{B}_{\Gamma_f} \left(\theta\, \mathbf{f}^{(i+1)} + (1-\theta)\, \mathbf{f}^{(i)}\right),$$

and the boundary matrix $\mathbf{B}_{\Gamma_f}$ given by:

$$\mathbf{B}_{\Gamma_f,kj} = \int_{\Gamma_f} \psi_j \, \varphi_k \, \mathrm{d}\mathbf{x}. \tag{1.33}$$

Note, incorporating the Neumann boundary conditions in the weak form corresponds to the following exchange of the boundary matrices $\mathbf{B}_\sigma$ and $\mathbf{B}_{\Gamma_f}$:

$$\mathbf{B}_\sigma \, \mathbf{u} = \mathbf{B}_{\Gamma_f} \, \mathbf{f}. \tag{1.34}$$

Equation (1.32) is used to solve the diffusion part of the monodomain equation given in Eq. (1.11) after inserting the corresponding constant prefactors.

When deriving or implementing new models or optimizing solver code, it is often beneficial to study certain effects in isolation. It can help to use a toy problem such as the simple Laplace problem $\Delta u = 0$, possibly with Neumann boundary condition $\partial u / \partial \mathbf{n} = f$. By specializing the formulation in Eq. (1.32) accordingly, we obtain the system

$$(\mathbf{K}_\mathrm{I} + \mathbf{B}_\mathrm{I}) \, \mathbf{u} = \mathbf{0}$$

for the case without boundary condition (set $\mathbf{B}_\mathrm{I}$ to zero to assume homogenous Neumann boundaries) or

$$\mathbf{K}_\mathrm{I} \, \mathbf{u} + \mathbf{B}_{\Gamma_f} \, \mathbf{f} = 0 \tag{1.35}$$

to include the formulated Neumann boundary condition.

1.2.3 Using Mass Lumping for Implicit Timestepping

Implicit timestepping schemes such as implicit Euler or the Crank-Nicoloson scheme for $\theta = \frac{1}{2}$ need to solve a linear equation in every timestep. Assuming homogeneous Neumann boundary conditions for simplicity, the iteration step of the canonical Crank-Nicolson scheme follows from Eq. (1.32):

$$\left(\frac{1}{2}\mathbf{K} - \frac{1}{dt}\mathbf{M}\right) \mathbf{u}^{(t+1)} = \left(-\frac{1}{2}\mathbf{K} - \frac{1}{dt}\mathbf{M}\right) \mathbf{u}^{(t)} \tag{1.36a}$$

$$\Leftrightarrow \quad (\mathbf{I} - \frac{dt}{2}\,\mathbf{M}^{-1}\mathbf{K})\,\mathbf{u}^{(t+1)} = \mathbf{u}^{(t)}(\mathbf{I} + \frac{dt}{2}\,\mathbf{M}^{-1}\mathbf{K}). \tag{1.36b}$$

For the implicit Euler method, we obtain:

$$(\mathbf{K} - \frac{\mathbf{M}}{dt})\,\mathbf{u}^{(t+1)} = -\frac{\mathbf{M}}{dt}\mathbf{u}^{(t)} \tag{1.37a}$$

$$\Leftrightarrow \quad (\mathbf{I} - dt\,\mathbf{M}^{-1}\mathbf{K})\,\mathbf{u}^{(t+1)} = \mathbf{u}^{(t)}. \tag{1.37b}$$

Both iteration steps in Equations (1.36a) and (1.36b) and in Equations (1.37) and (1.37a) are equivalent, as the second equation follows from the first one by left multiplication of $(-dt\mathbf{M}^{-1})$. In the second equations, the matrices to be multiplied with are created by a sum of the unity matrix $\mathbf{I}$ and another matrix term that is scaled by the potentially small timestep width dt. For the implicit Euler in Eq. (1.37b), the matrix on the right hand side even completely vanishes. This is preferred over the first iteration steps in Equations (1.36a) and (1.37a) as it leads to better conditioned matrix-vector multiplications.

The required inversions of the mass matrix cannot be carried out explicitly as the inversion would fill in numerous matrix entries and eliminate the sparse structure and this is not feasible for highly resolved meshes. Instead, mass lumping is used, where the mass matrix $\mathbf{M}$ is approximated by a diagonal matrix with diagonal entries equal to the row sums in $\mathbf{M}$ [Hin76]. Thus, multiplication with the inverse mass matrix corresponds to rescaling of columns by the inverse lumped diagonal entries.

1.2.4 Discretization of the Multidomain Model

With the prerequisites of temporal discretization in Sec. 1.2.1 and the Finite Element formulation of a diffusion equation in Sec. 1.2.2, we can now discretize the multidomain model. Since this has not been previously done in literature using the Finite Element Method, the following derivation is more detailed.

The first multidomain equation given in Eq. (1.14) yields the following form after applying the Finite Element derivation in Eq. (1.32):

$$\left(\mathbf{K}_{\boldsymbol{\sigma}_e+\boldsymbol{\sigma}_i} + \mathbf{B}_{\boldsymbol{\sigma}_e+\boldsymbol{\sigma}_i}\right)\boldsymbol{\phi}_e + \sum_{k=1}^{N_{\mathrm{MU}}} f_r^k \left(\mathbf{K}_{\boldsymbol{\sigma}_i^k} + \mathbf{B}_{\boldsymbol{\sigma}_i^k}\right)\mathbf{V}_m^k = 0. \tag{1.38}$$

Here, $\boldsymbol{\phi}_e$ and $\mathbf{V}_m^k$ are the vectors of degrees of freedom for the extracellular potential ϕ_e and membrane voltage V_m^k of compartment k. The matrices are defined by Eq. (1.31) and do not yet include the boundary conditions.

The diffusion part of the second multidomain equation, Eq. (1.15), discretized with Crank-Nicolson, yields the system

$$\mathbf{A}\begin{pmatrix}\mathbf{V}_m^{k,(i+1)}\\ \boldsymbol{\phi}_e^{(i+1)}\end{pmatrix}=\mathbf{b}, \tag{1.39}$$

with the 1×2 system matrix $\mathbf{A}$ and right hand side vector $\mathbf{b}$ given by:

$$\mathbf{A}=\left[\frac{\theta}{A_m^k C_m^k}(\mathbf{K}_{\boldsymbol{\sigma}_i^k}+\mathbf{B}_{\boldsymbol{\sigma}_i^k})-\frac{1}{dt}\mathbf{M}\qquad \frac{\theta}{A_m^k C_m^k}(\mathbf{K}_{\boldsymbol{\sigma}_i^k}+\mathbf{B}_{\boldsymbol{\sigma}_i^k})\right], \tag{1.40a}$$

$$\mathbf{b}=\Big(\frac{\theta-1}{A_m^k C_m^k}(\mathbf{K}_{\boldsymbol{\sigma}_i^k}+\mathbf{B}_{\boldsymbol{\sigma}_i^k})-\frac{1}{dt}\mathbf{M}\Big)\mathbf{V}_m^{k,(i)}+\frac{\theta-1}{A_m^k C_m^k}(\mathbf{K}_{\boldsymbol{\sigma}_i^k}+\mathbf{B}_{\boldsymbol{\sigma}_i^k})\boldsymbol{\phi}_e^{(i)}. \tag{1.40b}$$

A separate instance of this equation holds for every compartment k. Again, the integrals over the boundary are still present in the $\mathbf{B}_{\boldsymbol{\sigma}_i^k}$ matrices. To resolve this and close the formulation, we have to consider the fluxes over the boundary of all involved unknowns and replace them using the boundary conditions.

One required boundary conditions to solve the multidomain model without body domain is given in Eq. (1.16a). The boundary condition for compartment k in terms of the intracellular potential ϕ_i^k,

$$(\boldsymbol{\sigma}_i^k\nabla\phi_i^k)\cdot\mathbf{n}_m=0\qquad\text{on }\partial\Omega_M, \tag{1.41}$$

is expressed in terms of the unknowns V_m^k and ϕ_e to yield the condition

$$(\boldsymbol{\sigma}_i^k\nabla V_m^k)\cdot\mathbf{n}_m=-(\boldsymbol{\sigma}_i^k\nabla\phi_e)\cdot\mathbf{n}_m=:p^k\qquad\text{on }\partial\Omega_M. \tag{1.42}$$

We define the value of this flux to be equal to a helper variable p^k. A second flux is formulated for he extracellular potential ϕ_e. We assign its value to the helper variable q:

$$(\boldsymbol{\sigma}_e\nabla\phi_e)\cdot\mathbf{n}_m=:q\qquad\text{on }\partial\Omega_M. \tag{1.43}$$

We can now express the flux value $\big((\boldsymbol{\sigma}_e+\boldsymbol{\sigma}_i)\nabla\phi_e\big)\cdot\mathbf{n}_m$, which occurs in the discretized first multidomain equation, Eq. (1.38), in terms of the variables p^k and q. Using Equa-

tions (1.41) and (1.42) and the relation $\phi_e = \phi_i^k - V_m^k$, we derive:

$$\big((\boldsymbol{\sigma}_e + \boldsymbol{\sigma}_i)\nabla\phi_e\big)\cdot\mathbf{n}_m = (\boldsymbol{\sigma}_e\nabla\phi_e)\cdot\mathbf{n}_m + (\boldsymbol{\sigma}_i\nabla\phi_e)\cdot\mathbf{n}_m = q - \sum_{k=1}^{N_{\mathrm{MU}}} f_r^k\, p^k. \tag{1.44}$$

We discretize the flux values p^k and q analogously to the Neumann boundary condition flux f in Sec. 1.2.2 and summarize the degrees of freedoms in vectors $\mathbf{p}^k$ and $\mathbf{q}$.

Next, we combine the flux values with the first and second multidomain equation. Plugging the generic relation Eq. (1.34) for boundary integral terms into the discretization of the first multidomain equation, Eq. (1.38), and using the derived flux values in Equations (1.42) and (1.44) leads in a first step to the following equation:

$$\mathbf{K}_{\boldsymbol{\sigma}_e+\boldsymbol{\sigma}_i}\boldsymbol{\phi}_e + \mathbf{B}_{\Gamma_M}\big(\mathbf{q} - \sum_{k=1}^{N_{\mathrm{MU}}} f_r^k\,\mathbf{p}^k\big) + \sum_{k=1}^{N_{\mathrm{MU}}} f_r^k\big(\mathbf{K}_{\boldsymbol{\sigma}_i^k}\mathbf{V}_m^k + \mathbf{B}_{\Gamma_M}\mathbf{p}^k\big) = 0.$$

It can be seen that the terms involving $\mathbf{p}^k$ cancel out and result in:

$$\mathbf{K}_{\boldsymbol{\sigma}_e+\boldsymbol{\sigma}_i}\boldsymbol{\phi}_e + \sum_{k=1}^{N_{\mathrm{MU}}} f_r^k\mathbf{K}_{\boldsymbol{\sigma}_i^k}\mathbf{V}_m^k = -\mathbf{B}_{\Gamma_M}\mathbf{q}. \tag{1.45}$$

If the multidomain description is used without body fat domain, the boundary condition in Eq. (1.16b) is assumed and the right hand side in Eq. (1.45) vanishes. If a body domain is considered, the right hand side interacts with the body domain model.

Adding boundary conditions to the discretization of the second multidomain equation proceeds using Equations (1.39) and (1.40). Carrying out the analogous procedure to the first multidomain equation, we plug in Eq. (1.34) to yield the matrix equation

$$\mathbf{A}\begin{pmatrix}\mathbf{V}_m^{k,(i+1)}\\ \boldsymbol{\phi}_e^{(i+1)}\end{pmatrix} = \mathbf{b}, \tag{1.46}$$

with system matrix $\mathbf{A}$ and right hand side vector $\mathbf{b}$ given by:

$$\mathbf{A} = \left[\frac{\theta}{A_m^k C_m^k} \mathbf{K}_{\sigma_i^k} - \frac{1}{dt} \mathbf{M} \qquad \frac{\theta}{A_m^k C_m^k} \mathbf{K}_{\sigma_i^k}, \right], \tag{1.47}$$

$$\begin{aligned} \mathbf{b} = & \left(\frac{\theta - 1}{A_m^k C_m^k} \mathbf{K}_{\sigma_i^k} - \frac{1}{dt} \mathbf{M} \right) \mathbf{V}_m^{k,(i)} + \frac{\theta - 1}{A_m^k C_m^k} \mathbf{K}_{\sigma_i^k} \boldsymbol{\phi}_e^{(i)} \\ & + \frac{\theta - 1}{A_m^k C_m^k} \mathbf{B}_{\Gamma_M} \mathbf{p}^{k,(i)} - \frac{\theta - 1}{A_m^k C_m^k} \mathbf{B}_{\Gamma_M} \mathbf{p}^{k,(i)} - \frac{\theta}{A_m^k C_m^k} \mathbf{B}_{\Gamma_M} \mathbf{p}^{k,(i+1)} + \frac{\theta}{A_m^k C_m^k} \mathbf{B}_{\Gamma_M} \mathbf{p}^{k,(i+1)}. \end{aligned}$$

Again, the boundary terms involving $\mathbf{p}^k$ vanish to yield the following expression for $\mathbf{b}$:

$$\mathbf{b} = \left(\frac{\theta - 1}{A_m^k C_m^k} \mathbf{K}_{\sigma_i^k} - \frac{1}{dt} \mathbf{M} \right) \mathbf{V}_m^{k,(i)} + \frac{\theta - 1}{A_m^k C_m^k} \mathbf{K}_{\sigma_i^k} \boldsymbol{\phi}_e^{(i)}. \tag{1.48}$$

In summary, Eq. (1.45) with $\mathbf{q} = \mathbf{0}$ coupled with N_{MU} instances of Equations (1.46) to (1.48) comprise the discretization for the multidomain model without body domain. Definitions of the contained stiffness and mass matrices are given in Eq. (1.31).

1.2.5 Discretization of the Multidomain Model With Body Domain

To discretize the multidomain model with body domain, we reuse the formulation without body domain in Sec. 1.2.4. The body domain adds the electric potential ϕ_b to the unknowns that have to be solved. As before, we discretize the field using Finite Element ansatz functions and yield the vector $\boldsymbol{\phi}_b$ of degrees of freedom. The model for ϕ_b is the Laplace equation given in Eq. (1.17) with homogeneous Neumann boundary conditions given in Eq. (1.19). According to Eq. (1.35), the discretized equation is given by

$$\mathbf{K}_{\sigma_b} \boldsymbol{\phi}_b = 0. \tag{1.49}$$

The value of the body potential ϕ_b is coupled to the extracellular potential ϕ_e in the muscle domain Ω_M via the coupling conditions on the boundary Γ_M given in Eq. (1.18).

We combine the discretized and coupled multidomain equations into one linear system

of equations:

$$\left[\begin{array}{c|c|c|c} \mathbf{A}^k_{V_m,V_m} & \mathbf{B}^k_{V_m,\phi_e} & & \\ \mathbf{B}^k_{\phi_e,V_m} & \mathbf{B}_{\phi_e,\phi_e} & & \mathbf{B}_{\Gamma_M} \\ \hline & & \mathbf{C}_{\phi_b,\phi_b} & -\mathbf{B}_{\Gamma_M} \\ \hline & \mathbf{I}_{\Gamma_M,\phi_e} & -\mathbf{I}_{\Gamma_M,\phi_b} & \end{array}\right] \left[\begin{array}{c} \mathbf{V}_m^{k,(i+1)} \\ \hline \boldsymbol{\phi}_e^{(i+1)} \\ \hline \boldsymbol{\phi}_b^{(i+1)} \\ \hline \mathbf{q}^{(i+1)} \end{array}\right] = \left[\begin{array}{c} \mathbf{b}^{k,(i)}_{V_m} \\ \hline \mathbf{0} \\ \hline \mathbf{0} \\ \hline \mathbf{0} \end{array}\right]. \tag{1.50}$$

The vector of unknowns consists of the degrees of freedom in the Finite Element formulation at the next timestep $(i+1)$ of the transmembrane voltage $\mathbf{V}^{(i+1)}$, the extracellular potential $\boldsymbol{\phi}_e^{(i+1)}$, the body potential $\boldsymbol{\phi}_b^{(i+1)}$ and additionally the flux $\mathbf{q}^{(i+1)}$ over the shared boundary Γ_M of muscle and body domain, which was defined in Eq. (1.43). For illustration purposes, only one compartment, $k = 1$, for one MU, $N_{\text{MU}} = 1$, is considered.

The resulting matrix equation is organized in sub blocks, as shown in Eq. (1.50). In the following text, we refer to them as block rows and block columns.

The first block row in the matrix equation is given by the discretized second multidomain equation. Following Equations (1.47) and (1.48), the matrices and right hand side are given by:

$$\mathbf{A}^k_{V_m,V_m} = \frac{\theta}{A_m^k C_m^k}\mathbf{K}_{\boldsymbol{\sigma}_i^k} - \frac{1}{dt}\mathbf{M}, \qquad \mathbf{B}^k_{V_m,\phi_e} = \frac{\theta}{A_m^k C_m^k}\mathbf{K}_{\boldsymbol{\sigma}_i^k},$$

$$\mathbf{b}^{k,(i)}_{V_m} = \Big(\frac{\theta-1}{A_m^k C_m^k}\mathbf{K}_{\boldsymbol{\sigma}_i^k} - \frac{1}{dt}\mathbf{M}\Big)\mathbf{V}_m^{k,(i)} + \frac{\theta-1}{A_m^k C_m^k}\mathbf{K}_{\boldsymbol{\sigma}_i^k}\boldsymbol{\phi}_e^{(i)}.$$

The second block row describes the first multidomain equation that was derived in Eq. (1.45). The flux term $\mathbf{q}$ has been brought to the left hand side and is incorporated by the boundary matrix $\mathbf{B}_{\Gamma_M}$ defined in Eq. (1.33). The other matrices are formulated as follows:

$$\mathbf{B}^k_{\phi_e,V_m} = f_r^k \mathbf{K}_{\boldsymbol{\sigma}_i^k}, \qquad \mathbf{B}_{\phi_e,\phi_e} = \mathbf{K}_{\boldsymbol{\sigma}_e+\boldsymbol{\sigma}_i}$$

The third block row is the formulation of the harmonic body potential ϕ_b and the matrix $\mathbf{C}_{\phi_b,\phi_b}$ equals to the system matrix $\mathbf{K}_{\boldsymbol{\sigma}_b}$ in Eq. (1.49). The coupling condition on the flux q in Eq. (1.18b) is accounted for by including the boundary matrix $\mathbf{B}_{\Gamma_M}$ in the last column. The minus sign comes from the fact that the outward normal vector on Γ_M as the boundary of Ω_B is has the opposite direction to the normal vector on Γ_M that

is used for the models in the muscle domain Ω_M. Using the helper variable $\mathbf{q}^{(i+1)}$, the second and third row of Eq. (1.50) are coupled according to the prescribed condition in Eq. (1.18b).

The other coupling condition, Eq. (1.18a), is accounted for by the last row of blocks in Eq. (1.49). The degrees of freedom for the extracellular potential $\boldsymbol{\phi}_e^{(i+1)}$ and the body potential $\boldsymbol{\phi}_b^{(i+1)}$ have equal values on the boundary Γ_M. The matrices $\mathbf{I}_{\Gamma_M,\phi_e}$ and $\mathbf{I}_{\Gamma_M,\phi_b}$ are identity matrices that only have nonzero entries on the diagonal for the boundary degrees of freedom in the meshes of muscle domain and body domain, respectively.

Because the vector $\mathbf{q}^{(i+1)}$ is not an unknown in the system, the respective values in Eq. (1.50) have to be condensed out. In result, we obtain the following system, which is formulated for a generic number N_{MU} of MUs:

$$\left[\begin{array}{ccc|c|c} \mathbf{A}^1_{V_m,V_m} & & & \mathbf{B}^1_{V_m,\phi_e} & \\ & \ddots & & \vdots & \\ & & \mathbf{A}^{N_{\mathrm{MU}}}_{\phi_e,V_m} & \mathbf{B}^{N_{\mathrm{MU}}}_{V_m,\phi_e} & \\ \mathbf{B}^1_{\phi_e,V_m} & \dots & \mathbf{B}^{N_{\mathrm{MU}}}_{\phi_e,V_m} & \mathbf{B}_{\phi_e,\phi_e} & \mathbf{D} \\ \hline & & & \mathbf{E} & \tilde{\mathbf{C}}_{\phi_b,\phi_b} \end{array}\right] \left[\begin{array}{c} \mathbf{V}_m^{1,(i+1)} \\ \vdots \\ \mathbf{V}_m^{N_{\mathrm{MU}},(i+1)} \\ \hline \boldsymbol{\phi}_e^{(i+1)} \\ \hline \tilde{\boldsymbol{\phi}}_b^{(i+1)} \end{array}\right] = \left[\begin{array}{c} \mathbf{b}_{V_m}^{1,(i)} \\ \vdots \\ \mathbf{b}_{V_m}^{N_{\mathrm{MU}},(i)} \\ \mathbf{0} \\ \hline \mathbf{0} \end{array}\right]. \tag{1.51}$$

Formally, the condensation step is carried out by adding the equations of the third block row in Eq. (1.51) that correspond to the boundary degrees of freedom on Γ_M to the corresponding equations of the same dofs in the second block row. This eliminates the last block column, which corresponds to $\mathbf{q}^{(i+1)}$. Next, the duplicate boundary dofs that appear in both the Ω_M and Ω_B meshes get unified. The corresponding matrix columns in the third block column are removed. To preserve the entries in the third block row, they are added in the sub matrix of block row three and block column two.

Now considering the updated matrix equation in Eq. (1.51), all sub blocks are equal to Eq. (1.50), except for the former matrix $\mathbf{C}_{\phi_b,\phi_b}$ and the new matrices $\mathbf{D}$ and $\mathbf{E}$. The new matrix $\tilde{\mathbf{C}}_{\phi_b,\phi_b}$ is obtained from $\mathbf{C}_{\phi_b,\phi_b}$ by removing all rows and columns of boundary degrees of freedom. The removed entries are contained in the new matrices $\mathbf{D}$ and $\mathbf{E}$.

The size of the system matrix in Eq. (1.51) equals $a \times a$, where the number a is composed of $N_{\mathrm{MU}} + 1$ times the number of degrees of freedom in the muscle mesh plus the number of degrees of freedom in the fat layer mesh without the boundary degrees of freedom on Γ_M. Accordingly, the vector $\tilde{\boldsymbol{\phi}}_b^{(i+1)}$ is the same as $\boldsymbol{\phi}_b^{(i+1)}$ except that it does not contain the boundary degrees of freedom, which are already included in $\boldsymbol{\phi}_e^{(i+1)}$.

Equation (1.51) describes one iteration of the Crank-Nicolson scheme that is needed for solving the multidomain model. This iteration is carried out alternatingly with the subcellular model, according to the chosen operator splitting scheme. Equation (1.51) contains the second multidomain equation for every MU in the first N_{MU} block rows, the first multidomain equation in the second-to-last block row and the body fat layer model in the last block row. Because of this implicit formulation, electric conduction in the intra and extracellular space and the body domain are bidirectionlly coupled. Therefore, the model can be used to simulate the effects of natural activation in the muscle on EMG signals on the skin surface as well as the effects of external stimulation on the surface on the electrophysiology.

1.2.6 Summary of Domains and Meshes

Finite Element meshes need to be created for the 1D fiber domains Ω_f^j for $j = 1, \ldots, n$ if the fiber based description is used and for the 3D muscle domain Ω_M and the 3D body domain Ω_B. The meshes for Ω_M and Ω_B have to share nodes on the common boundary Γ_M. The fiber meshes are embedded in the muscle domain. Their nodes do not necessarily have to coincide with the nodes of the muscle mesh.

The subcellular model is solved at locations Ω_s^i for $i = 1, \ldots, m$. These locations are the nodes of the fiber meshes for the fiber based description and the nodes of the muscle mesh for the multidomain description. We therefore have the inclusion $\Omega_s^i \subset \Omega_f^j \subset \Omega_M$.

For the solid mechanics model, the unified 3D domain $\Omega = \Omega_M \cup \Omega_B$ is used. The mesh for the continuum mechanics formulation can be different from the meshes used for the electrophysiology model. In fact, the continuum mechanics mesh has special requirements in order to yield a consistent formulation, e.g., our implementation uses two overlayed meshes of quadratic and linear hexahedral elements for displacements and the hydrostatic pressure. Often, the required accuracy of the electrophysiology model is higher than for the continuum mechanics model such that differently resolved meshes can be used. To facilitate data mapping, the nodes of the mechanics mesh should be chosen as subset of the nodes of the electrophysiology meshes.

1.3 Discretization and Solution of the Solid Mechanics Model

The following section describes the Finite Element discretization of the solid mechanics model and the algorithmic solution. Dynamic finite elasticity methods considering large strains and a generic hyperelastic materials, both incompressible and compressible, are less frequently used than linear elasticity descriptions, which involve linearizations at various levels. However, corresponding formulations exist in the literature with partly varying conventions and symbols. Our implementation of a solver for such a generic descripton enabling instruction-level and shared-memory parallelism and being usable for a multi-scale biomechanics model is an interdisciplinary endeavour. Therefore, we summarize the required basics and the derivation up to the final algorithm such that it may serve also readers that are not specialized in the field of continuum mechanics. The derivation largely follows the book of Holzapfel [Hol00], the discretization follows the work of Zienkiewicz, Taylor et al. [Zie77]; [Zie05].

1.3.1 Geometric Description

We begin with the geometric description of the material body and define the basic quantities that are later used to describe the physics. As introduced in Sec. 1.1.6, the placement function $\chi_t : \Omega_0 \rightarrow \Omega_t$ maps points $\mathbf{X}$ in reference configuration Ω_0 to points $\mathbf{x} = \mathbf{X} + \mathbf{u}$ in the current configuration Ω_t using the displacement field $\mathbf{u}$.

The deformation gradient $\mathbf{F}$ is the second order tensor that is obtained by deriving the placement function. It is given using the unit vectors $\mathbf{e}_i$ and components F_{ij}:

$$\mathbf{F} = F_{ij}\, \mathbf{e}_i \otimes \mathbf{e}_j, \qquad F_{ij} = \frac{\partial x_i}{\partial X_j}.$$

The deformation gradient can also be expressed using the displacement field $\mathbf{u}$:

$$\mathbf{F} = \mathbf{I} + \nabla \mathbf{u}. \tag{1.52}$$

Here and in the following, the gradient symbol ∇ refers to differentiation with respect to material coordinates $\mathbf{X}$. We assume cartesian coordinates such that the metric tensor $\mathbf{g}$ that occurs, e.g., in the transformation from tangent to co-tangent space equals the identity and can be omitted. This simplifies the description.

The determinant of the deformation gradient is $J := \det \mathbf{F} > 0$. Is is positive for any valid transformation. The deformation gradient is used to map geometric quantities from reference to current configuration:

$$\mathbf{t} = \mathbf{F}\,\mathbf{T}, \qquad \text{(tangent map)} \tag{1.53a}$$

$$\mathbf{a} = \operatorname{cof}(\mathbf{F})\,\mathbf{A}, \qquad \text{(normal map)} \tag{1.53b}$$

$$v = J\,V. \qquad \text{(volume map)} \tag{1.53c}$$

The tensor $\mathbf{F}$ maps material tangents $\mathbf{T}$ in Ω_0 to the corresponding spatial line elements in $\mathbf{t}$ in Ω_t as given in Eq. (1.53a) and visualized in Fig. 1.5. The spatial stretch at a point $\mathbf{x} \in \Omega_t$ in a certain direction is given by $\lambda = \sqrt{\boldsymbol{\lambda}^\top \boldsymbol{\lambda}}$ with $\boldsymbol{\lambda} = \mathbf{F}\,\mathbf{M}$, where $\mathbf{M}$ is a material line element with unit length pointing in the respective Lagrangian direction.

In Eq. (1.53b), the cofactor of $\mathbf{F}$ given by $\operatorname{cof}(\mathbf{F}) = J\,\mathbf{F}^{-\top}$ maps normals $\mathbf{A}$ and surface areas $|\mathbf{A}|$ from Ω_0 to the corresponding values $\mathbf{a}$ and $|\mathbf{a}|$ in Ω_t. Nanson's formula, $\mathrm{d}\mathbf{a} = \operatorname{cof}(\mathbf{F})\,\mathrm{d}\mathbf{A}$, is used to transform surface integrals from Eulerian to Lagrangian description. Note that tangents and normals at a point $\mathbf{X}$ live in the tangent space $T_{\mathbf{X}}\Omega_0$ and co-tangent space $T^*_{\mathbf{X}}\Omega_0$, respectively. Equation (1.53c) lists the volume map from Ω_0 to Ω_t that simply scales the volume by the determinant J.

Furthermore, the deformation gradient $\mathbf{F}$ is used to define the right Cauchy Green tensor $\mathbf{C} = \mathbf{F}^\top \mathbf{F}$, which maps from tangent to co-tangent space in reference configuration and subsequently the Green-Lagrange strain tensor:

$$\mathbf{E} = \frac{1}{2}(\mathbf{C} - \mathbf{I}).$$

This strain measure can be interpreted as comparing the current Lagrangian metric $\mathbf{C}$, which is a measure for the symmetric part of the current deformation, with the reference metric which is the identity. Using Eq. (1.52), the Green-Lagrange strain tensor can be formulated only in terms of derivatives of the displacements:

$$\mathbf{E} = \frac{1}{2}\left((\nabla \mathbf{u})^\top + \nabla \mathbf{u}\right) + \frac{1}{2}\nabla \mathbf{u}^\top \nabla \mathbf{u}. \tag{1.54}$$

To employ the physical balance principles described in Sec. 1.1.6, we need to define stress measures. The cauchy stress tensor $\boldsymbol{\sigma}$ has been introduced using Euler's cut principle where the mechanical action on an arbitrary cut out of the domain is represented by a traction vector $\mathbf{t}$, i.e. a contact force per surface area. The traction vector acts on the

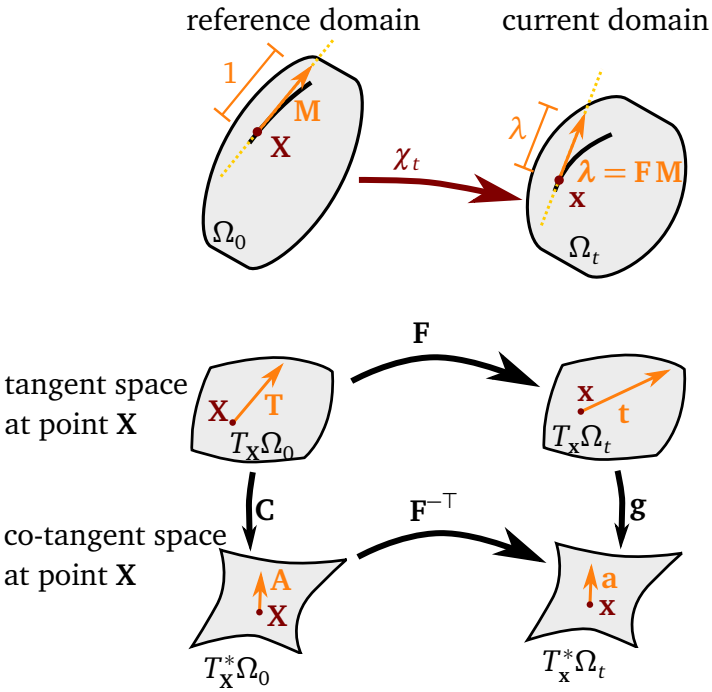

Figure 1.5: Vector spaces and variables used in the geometric description for the solid mechanics model. The left side shows the reference domain with tangent and co-tangent space of point **X**. The right side shows these space for the current domain and a point **x**. The maps χ_t, **F** and $\mathbf{F}^{-\top}$ map tangents and normals between the configurations.

current configuration and is a function of the position $\mathbf{x} \in \Omega_t$ and the local orientation of the cut given by the normal vector **n**. Then, dhe stress tensor $\boldsymbol{\sigma}$ is defined by Cauchy's theorem:

$$\mathbf{t} = \boldsymbol{\sigma} \cdot \mathbf{n}$$

Thus, the Cauchy stress describes the "true stress" of contact forces per deformed area. Both slots of the second order tensor are associated with the current configuration, more specifically σ is contravariant and maps from a normal **n** in co-tangent space $T^*_{\mathbf{x}}\Omega_t$ to the traction **t** in tangent space $T_{\mathbf{x}}\Omega_t$. While the physical description is natural in this Eulerian setting, the numerical treatment is more convenient in the Lagrangian setting, where we can integrate over a non-deforming domain. In engineering, a two-point setting is often useful where surface areas are measured in the undeformed configuration and traction forces are measured in the deformed configuration. This is natural, e.g., in stretch experiments. Therefore, other stress measures involving the reference configuration are defined.

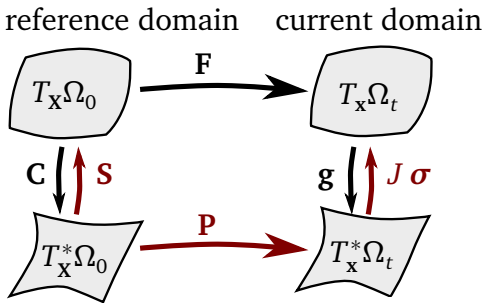

Figure 1.6: Stress tensors and geometric maps that can be used together in a solid mechanics formulation. The right Cauchy-Green tensor $\mathbf{C}$ and the second Piola-Kirchhoff stress $\mathbf{S}$ are dual Eulerian tensors and map between tangent space $T_X\Omega_0$ and co-tangent space $T^*_X\Omega_0$ in the reference domain. The deformation gradient $\mathbf{F}$ and the first Piola-Kirchhoff stress $\mathbf{P}$ are dual two-point tensors mapping from reference to current configuration. The Eulerian metric $\mathbf{g}$ which is the identity in cartesian coordinates and the Kirchhoff stress $J\,\boldsymbol{\sigma}$ (where $\boldsymbol{\sigma}$ is the Cauchy stress) are the dual objects in the Eulerian setting. All three pairs of dual tensors are linked together by transformations such as pull-back and push-forward.

Using the mappings presented in Eq. (1.53), all quantities can be transformed between both configurations. The physical derivation can be carried out equivalently in a Lagrangian or Eulerian setting and switching between them is possible at any point in the derivation. For this purpose two operations are defined, the pull-back $\varphi^*(\mathbf{g}) = \mathbf{F}^\top \mathbf{g}\,\mathbf{F}$ and push-forward $\varphi_*(\mathbf{G}) = \mathbf{F}^{-\top}\mathbf{G}\,\mathbf{F}^{-1}$, which bring tensors from Eulerian to Lagrangian description and vice-versa.

The first Piola-Kirchhoff stress tensor $\mathbf{P}$ measures contact forces in current configuration with regard to the area of the reference configuration and relates to the Cauchy stress as $\mathbf{P} = \boldsymbol{\sigma}\,\mathrm{cof}(\mathbf{F})$. The second Piola-Kirchhoff tensor $\mathbf{S}$ is a fully Lagrangian field given as the pull-back of the Cauchy stress scaled by J:

$$\mathbf{S} = \varphi^*(J\,\boldsymbol{\sigma}) = J\,\mathbf{F}^{-1}\boldsymbol{\sigma}\,\mathbf{F}^{-\top}.$$

Figure 1.6 summarizes the geometric maps by black arrows and the stress measures by red arrows. To relate strains and stresses in a material model, the corresponding tensors have to be dual objects. Here, three settings are possible: The Eulerian setting uses the metric $\mathbf{g}$ and the dual Kirchhoff stress $J\,\boldsymbol{\sigma}$. The two-point setting uses the deformation gradient $\mathbf{F}$ and the dual first Piola-Kirchhoff stress $\mathbf{P}$. The Lagrangian setting uses the right Cauchy-Green tensor $\mathbf{C}$ and the dual second Piola-Kirchhoff stress $\mathbf{S}$. For further derivations, we consider the Lagrangian setting.

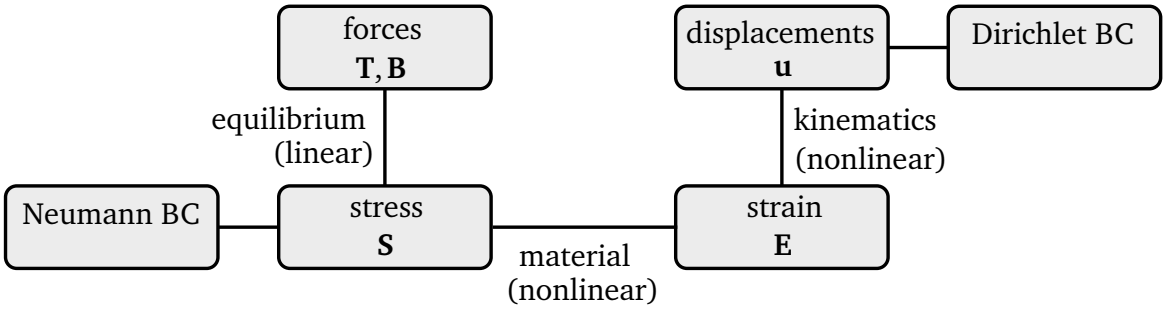

Figure 1.7: The three relations between various quantities that compose the solid mechanics model: Equilibrium links traction and body forces **T** and **B** to the stresses **S**. A material model connects them to strains **E**. The kinematic relations yield the resulting displacement field **u**. Note that all quantities in this diagram are given in Lagrangian formulation.

1.3.2 A Linearized Model as an Examplary Description of Solid Mechanics

The quantities that were introduced in Sec. 1.3.1 are linked together by the relations presented in Fig. 1.7. The goal is to find the relation between given forces (top left in Fig. 1.7) and the resulting deformation of the body described by the displacement (top right in Fig. 1.7). Prescribed external traction forces **T** and external or inertial body forces **B** act on the body and result in stresses **S** satisfying the equilibrium relation. A material law connects stresses **S** and strains **E**. The kinematics of the body determine the relationship between displacements **u** and strains **E**. Geometric dirichlet boundary conditions prescribe displacements and Neumann boundary conditions such as traction forces contribute to the stress field.

Whereas the equilibrium relation is linear, the material and kinematics descriptions can both be chosen to be linear or nonlinear. In cases of small strains geometric and material linearity can be assumed. In the following, we present a simplified, static model where all these relations are linear. This serves as a prototype for the later derivation of the fully nonlinear model. Our software OpenDiHu also implements this linear model. It exhibits better numerical properties and can be solved faster than the generic model. Thus, it can serve as a toy problem and for mechanical systems where the linearization assumption is valid.

Using variational calculus, the system response of external forces and infinitesimal, compatible, virtual displacements $\delta\mathbf{u}$ is studied. We start with the principle of virtual work which states that in equilibrium the virtual work δW performed by external forces

along virtual displacements $\delta\mathbf{u}$ is zero. Equivalently, the internal virtual work δW_{int} is equal to the external virtual work δW_{ext}. The external virtual work δW_{ext} is given by external forces $\mathbf{t}$ and the virtual displacements $\delta\mathbf{u}$ at the same location. The internal virtual work δW_{int} is the body's response in terms of stresses $\boldsymbol{\sigma}$ and virtual strains $\boldsymbol{\varepsilon}$. In summary, the equilibrium equation is given by:

$$\delta W_{\text{int}}(\mathbf{u}, \delta\mathbf{u}) = \delta W_{\text{ext}}(\delta\mathbf{u}) \qquad \forall \delta\mathbf{u} \in H_0^1(\Omega) \tag{1.55}$$

$$\Leftrightarrow \quad \int_\Omega \boldsymbol{\sigma}(\mathbf{u}) : \delta\boldsymbol{\varepsilon}\, \mathrm{d}\mathbf{x} = \int_{\partial\Omega} \mathbf{t} : \delta\mathbf{u}\, \mathrm{d}\mathbf{x} \qquad \forall \delta\mathbf{u} \in H_0^1(\Omega). \tag{1.56}$$

Here, the vectors contain the degrees of freedom of a Finite Element discretization. The operator ":" denotes the component-wise product. Often, it is easier to write the equations in component form. Indices $a, b, c, \ldots$ are used to specify a dimensionality index in $\{1, \ldots, d\}$. Capital letters $L, M \in \{1, \ldots, N\}$ designate indices over degrees of freedom in a mesh with N nodes. The Einstein sum convention is used where repeated indices implicitly indicate summation, except when the indices are in parantheses. Thus, the right hand side of Eq. (1.55) with ansatz functions ϕ^L and the degrees of freedom δu_a^L of $\delta\mathbf{u}$ can be written as:

$$\mathbf{f}_a = \int_{\partial\Omega} t_{(a)}\, \delta u_{(a)}^L\, \phi^L\, \mathrm{d}\mathbf{x}.$$

The linear material model is Hooke's law, given by

$$\boldsymbol{\sigma} = \mathbb{C} : \boldsymbol{\varepsilon} \tag{1.57}$$

with the forth order material tensor

$$\mathbb{C}_{abcd} = K\, \delta_{ab}\, \delta_{cd} + \mu(\delta_{ac}\, \delta_{bd} + \delta_{ad}\, \delta_{bc} - \frac{2}{3}\, \delta_{ab}\, \delta_{cd}).$$

The bulk modulus K is a measure for the (in-)compressibility and the shear modulus μ specifies the elastic shear stiffness. δ_{ab} is the Kronecker delta. The material tensor $\mathbb{C}$ exhibits the following major and minor symmetries:

$$\mathbb{C}_{abcd} = \mathbb{C}_{cdab}, \qquad \text{(major symmetries)} \tag{1.58a}$$

$$\mathbb{C}_{abcd} = \mathbb{C}_{bacd} = \mathbb{C}_{abdc} = \mathbb{C}_{badc}, \qquad \text{(minor symmetries)} \tag{1.58b}$$

effectively reducing the number of independent entries from 81 to 21 for 3D domains.

The third relation according to Fig. 1.7 is the kinematics relation between displacements $\mathbf{u}$ and strains $\boldsymbol{\varepsilon}$. The strain expression given in Eq. (1.54) is linearized by neglecting the higher order terms:

$$\boldsymbol{\varepsilon} = \frac{1}{2}\left((\nabla \mathbf{u})^{\top} + \nabla \mathbf{u}\right). \tag{1.59}$$

Because of small displacements, we do not distinguish between reference and current configuration as Eq. (1.55) combines the strain measure $\boldsymbol{\varepsilon}$, which is derived from the Lagrangian Green-Lagrange strain with the Eulerian Cauchy stress $\boldsymbol{\sigma}$.

By combining Equations (1.55), (1.57), and (1.59) and discretizing displacements and virtual displacements, we get the linear matrix equation

$$\mathbf{K}\,\mathbf{u} = \mathbf{f}. \tag{1.60}$$

The stiffness matrix $\mathbf{K}$ has rows and columns for every degree of freedom $L, M \in \{1, \ldots, N\}$ and the dimension indices $a, b \in \{1, 2, 3\}$:

$$\mathbf{K}_{LaMb} = \int_{\Omega} \mathbb{C}_{adbc} \frac{\partial \phi^{L}(\mathbf{x})}{\partial x_d} \frac{\partial \phi^{M}(\mathbf{x})}{\partial x_c} \, \mathrm{d}\mathbf{x}.$$

The resulting model in Eq. (1.60) describes the passive behaviour of a body under the linearization assumptions. For muscle tissue, we also need to incorporate active stresses that are generated at the sarcomeres in the muscle. We add an active stress term $\boldsymbol{\sigma}^{\text{active}}$ to the external virtual work in Eq. (1.55), yielding:

$$\delta W_{\text{int}}(\mathbf{u}, \delta\mathbf{u}) = \mathbf{f} + \int_{\Omega} \boldsymbol{\sigma}^{\text{active}} : \delta\boldsymbol{\varepsilon}_{-} \, \mathrm{d}\mathbf{x} \qquad \forall \delta\mathbf{u} \in H_0^1(\Omega). \tag{1.61}$$

The active stress is associated with compression, i.e., negative virtual strains $\delta\boldsymbol{\varepsilon} < 0$. Therefore, we use $\delta\boldsymbol{\varepsilon}_{-}$ which is defined equal to $\delta\boldsymbol{\varepsilon}$ for $\delta\boldsymbol{\varepsilon} < 0$ and zero otherwise. From Eq. (1.61), we get the same linear system as in Eq. (1.60) with an additional term $\mathbf{f}^{\text{active}}$ at the right hand side that contains the prescribed active stress field $\boldsymbol{\sigma}_{ab}^{\text{active}}(\mathbf{x})$:

$$\mathbf{f}_{La}^{\text{active}} = \int_{\Omega} \boldsymbol{\sigma}_{ab}^{\text{active}}(\mathbf{x}) \frac{\partial \phi^{L}(\mathbf{x})}{\partial x_b} \, \mathrm{d}\mathbf{x}.$$

1.3.3 Material Modeling

Next, the derivation for the nonlinear case is presented. We begin with the description of the material law which links strains and stresses. As noted in Sec. 1.3, the strain energy function ψ is used to define the material model. It is linked to the second Piola-Kirchhoff stress $\mathbf{S}$ by the relation

$$\mathbf{S} = 2\frac{\partial \Psi(\mathbf{C})}{\partial \mathbf{C}}. \tag{1.62}$$

The principle of material objectivity requires that material properties are invariant under a change of observer. As a result, the representation theorem for isotropic materials states that the stress tensor can be represented using three strain invariants I_1, I_2 and I_3. For a transversely isotropic material, the two invariants I_4 and I_5 that depend on an anisotropy direction $\mathbf{a}_0$ (corresponding to a fiber direction) are added.

Consequently, we can formulate the strain energy function $\Psi = \Psi(I_1, I_2, I_3, I_4, I_5)$ in terms of the strain invariants I_1 to I_5 of the right Cauchy Green tensor $\mathbf{C}$, which are defined as:

$$I_1(\mathbf{C}) = \mathrm{tr}\,(\mathbf{C}), \qquad I_2(\mathbf{C}) = \frac{1}{2}\left(\mathrm{tr}\,(\mathbf{C})^2 - \mathrm{tr}\,(\mathbf{C}^2)\right), \qquad I_3(\mathbf{C}) = \det(\mathbf{C}) = J^2,$$

$$I_4(\mathbf{C}, \mathbf{a}_0) = \mathbf{a}_0 \cdot \mathbf{C}\,\mathbf{a}_0, \qquad I_5(\mathbf{C}, \mathbf{a}_0) = \mathbf{a}_0 \cdot \mathbf{C}^2\,\mathbf{a}_0.$$

Note that incompressibility is equivalent to $J = 1$ and, thus, $I_3(\mathbf{C}) = 1$.

It is convenient to use a decoupled description where the deformation gradient $\mathbf{F}$ and the right Cauchy-Green tensor are multiplicatively decomposed into volume-changing (volumetric) and volume-preserving (isochoric) part:

$$\mathbf{F} = (J^{1/3}\mathbf{I})\,\bar{\mathbf{F}}, \qquad \mathbf{C} = (J^{2/3}\mathbf{I})\,\bar{\mathbf{C}}.$$

In consequence, the isochoric or distortional parts are given by

$$\bar{\mathbf{F}} = J^{-1/3}\,\mathbf{F}, \qquad \bar{\mathbf{C}} = J^{-2/3}\,\mathbf{C}.$$

The reduced invariants $\bar{I}_1$ to $\bar{I}_5$ are defined accordingly. Similarly, the strain energy function has a decoupled representation with volumetric part Ψ_{vol} and isochoric part

Ψ_{iso}:

$$\Psi = \Psi_{\text{vol}}(J) + \Psi_{\text{iso}}(\bar{\mathbf{C}}) = \Psi_{\text{vol}}(J) + \Psi_{\text{iso}}(\bar{I}_1, \bar{I}_2, \bar{I}_4, \bar{I}_5).$$

Any incompressible material can be modeled using the decoupled form and the penalty method as follows. The isochoric strain energy $\Psi_{\text{iso}}(\bar{\mathbf{C}})$ is given normally, e.g., by the Mooney-Rivlin model in Eq. (1.25). The volumetric part is defined as

$$\Psi_{\text{vol}}(J) = \kappa\, G(J), \qquad G(J) = \frac{1}{2}(J-1)^2,$$

with the incompressiblity parameter κ and the strictly convex penalty function $G(J)$ that approaches zero when reaching incompressiblity as J approaches 1. For large values of κ, the behavior is nearly incompressible. A disadvantage of this method is that the resulting system matrix is poorly conditioned and approaches a singularity for $J \to 1$. A better approach is to use a mixed formulation, where incompressiblity is enforced exactly using a Lagrange multiplier. This is also implemented in OpenDiHu and is the preferred method for incompressible materials. In OpenDiHu, the strain energy function of a new material can be given using any of the following four terms:

$$\Psi = \Psi_{\text{vol}}(J) + \Psi_{\text{iso}}(\bar{I}_1, \bar{I}_2, \bar{I}_4, \bar{I}_5) + \Psi_1(I_1, I_2, I_3) + \Psi_2(\mathbf{C}, \mathbf{a}_0)$$

The decoupled form is available with Ψ_{vol} and Ψ_{iso}, the coupled form for isotropic materials can be used via Ψ_1. The term Ψ_2 gives the most flexibility, as the constitutive model can be directly formulated using the right Cauchy-Green tensor $\mathbf{C}$ and the fiber direction $\mathbf{a}_0$. The unused terms can be defined as constant zero. The incompressiblity contraint using Lagrange multipliers can be switched on or off such that also compressible materials are possible.

1.3.4 Derivative of the stress tensor and elasticity tensor

Following Eq. (1.62), the second Piola-Kirchhoff stress $\mathbf{S}$ is given by a the derivative of the strain energy function Ψ with respect to $\mathbf{C}$. For the representation using the invariants, the chain rule has to be used:

$$\mathbf{S} = 2\frac{\partial \Psi(\mathbf{C})}{\partial \mathbf{C}} = \frac{\partial \Psi}{\partial I_a}\frac{\partial I_a}{\partial \mathbf{C}}.$$

Using the decoupled form, the resulting stresses are also decoupled as $\mathbf{S} = \mathbf{S}_{\text{vol}} + \mathbf{S}_{\text{iso}}$. The volumetric stress $\mathbf{S}_{\text{vol}}$ describes the elastic response to compression, the isochoric stress $\mathbf{S}_{\text{iso}}$ describes the response to the deviatoric deformation. In the following, all steps to compute these stresses are listed. The reasoning is to give a condensed reference of the implemented steps in OpenDiHu to facilitate further development. For the derivation of all intermediate steps, refer to the literature [Hol00].

At first, the reduced stress tensor $\bar{\mathbf{C}}$ is computed that neglects the volumetric change:

$$\bar{\mathbf{S}} = 2\frac{\partial \Psi_{\text{iso}}(\bar{I}_1, \bar{I}_2, \bar{I}_4, \bar{I}_5)}{\partial \bar{\mathbf{C}}} = \bar{\gamma}_1 \mathbf{I} + \bar{\gamma}_2 \bar{\mathbf{C}} + \bar{\gamma}_4 \mathbf{a}_0 \otimes \mathbf{a}_0 + \bar{\gamma}_5 (\mathbf{a}_0 \otimes \bar{\mathbf{C}} \mathbf{a}_0 + \mathbf{a}_0 \bar{\mathbf{C}} \otimes \mathbf{a}_0).$$

In case of an isotropic material, the terms with $\mathbf{a}_0$ are not needed. The factors are given by

$$\bar{\gamma}_1 = 2\left(\frac{\partial \Psi_{\text{iso}}(\bar{I}_1, \bar{I}_2)}{\partial \bar{I}_1} + \bar{I}_1 \frac{\partial \Psi_{\text{iso}}(\bar{I}_1, \bar{I}_2)}{\partial \bar{I}_2}\right), \quad \bar{\gamma}_2 = -2\frac{\partial \Psi_{\text{iso}}(\bar{I}_1, \bar{I}_2)}{\partial \bar{I}_2}, \quad \bar{\gamma}_4 = 2\frac{\partial \Psi_{\text{iso}}}{\partial \bar{I}_4}$$

$$\bar{\gamma}_5 = 2\frac{\partial \Psi_{\text{iso}}}{\partial \bar{I}_5}$$

Using the identity $\mathbb{I}$ and projection tensor $\mathbb{P}$,

$$(\mathbb{I})_{abcd} = \delta_{ac}\,\delta_{bd}, \qquad \mathbb{P} = \mathbb{I} - \frac{1}{3}\mathbf{C}^{-1} \otimes \mathbf{C},$$

the stress tensors can finally be computed:

$$\mathbf{S}_{\text{iso}} = J^{-2/3}\mathbb{P} : \bar{\mathbf{S}}, \qquad \mathbf{S}_{\text{vol}} = J\,p\,\mathbf{C}^{-1}, \qquad \mathbf{S} = \mathbf{S}_{\text{iso}} + \mathbf{S}_{\text{vol}}.$$

In the compressible case including the penalty method, the value of p is given by the constitutive model as $p = \mathrm{d}\Psi_{\text{vol}}(J)/\mathrm{d}J$. Otherwise, p is the unknown Lagrange multiplier that gets solved for. Then, p is identified as the hydrostatic pressure.

Another important quantity for the numerical solution is the forth order elasticity tensor $\mathbb{C}$ defined as

$$\mathbb{C} = 2\frac{\partial \mathbf{S}(\mathbf{C})}{\partial \mathbf{C}} = 4\frac{\partial^2 \Psi(\mathbf{C})}{\partial \mathbf{C} \partial \mathbf{C}}.$$

It is the derivative of the stress tensor and is required for the iterations of the nonlinear Newton solver. Like the material tensor in Eq. (1.58), it shows major and minor symmetries and has 21 independent entries.

Like the stress tensor, the elasticity tensor is also additively composed into a volumetric term $\mathbb{C}_{\text{vol}}$ and an isochoric term $\mathbb{C}_{\text{iso}}$. The volumetric term can be computed by:

$$\mathbb{C}_{\text{vol}} = J\,\tilde{p}\,\mathbf{C}^{-1}\otimes\mathbf{C}^{-1} - 2J\,p\,\mathbf{C}^{-1}\odot\mathbf{C}^{-1}, \quad \left(\mathbf{C}^{-1}\odot\mathbf{C}^{-1}\right)_{abcd} = \frac{1}{2}\left(C^{-1}_{ac}\,C^{-1}_{bd} + C^{-1}_{ad}\,C^{-1}_{bc}\right).$$

For the incompressible formulation, $\tilde{p}$ equals the Lagrange multiplier p. For the compressible formulation, it is derived as $\tilde{p} = p + J\,\mathrm{d}p/\mathrm{d}J$.

The isochoric term of the elasticity tensor follows from the following list of quantities to compute:

$$\bar{\delta}_1 = 4\left(\frac{\partial^2\Psi_{\text{iso}}}{\partial\bar{I}_1\,\partial\bar{I}_1} + 2\,\bar{I}_1\frac{\partial^2\Psi_{\text{iso}}}{\partial\bar{I}_1\,\partial\bar{I}_2} + \frac{\partial\Psi_{\text{iso}}}{\partial\bar{I}_2} + \bar{I}_1^2\frac{\partial^2\Psi_{\text{iso}}}{\partial\bar{I}_2\,\partial\bar{I}_2}\right),\ \bar{\delta}_2 = -4\left(\frac{\partial^2\Psi_{\text{iso}}}{\partial\bar{I}_1\,\partial\bar{I}_2} + \bar{I}_1\frac{\partial^2\Psi_{\text{iso}}}{\partial\bar{I}_2\,\partial\bar{I}_2}\right),$$

$$\bar{\delta}_3 = 4\frac{\partial^2\Psi_{\text{iso}}}{\partial\bar{I}_2\,\partial\bar{I}_2}, \quad \bar{\delta}_4 = -4\frac{\partial\Psi_{\text{iso}}}{\partial\bar{I}_2}, \quad \bar{\delta}_5 = 4\left(\frac{\partial^2\Psi_{\text{iso}}}{\partial\bar{I}_1\,\partial\bar{I}_4} + \bar{I}_1\frac{\partial^2\Psi_{\text{iso}}}{\partial\bar{I}_2\,\partial\bar{I}_4}\right),$$

$$\bar{\delta}_6 = -4\frac{\partial^2\Psi_{\text{iso}}}{\partial\bar{I}_2\,\partial\bar{I}_4}, \quad \bar{\delta}_7 = 4\frac{\partial^2\Psi_{\text{iso}}}{\partial\bar{I}_4\,\partial\bar{I}_4}, \quad \mathbb{I}_{abcd} = \delta_{ac}\,\delta_{bd}, \quad \bar{\mathbb{I}}_{abcd} = \delta_{ad}\,\delta_{bc}, \quad \mathbb{S} = (\mathbb{I}+\bar{\mathbb{I}})/2,$$

$$\frac{\partial\bar{I}_5}{\partial\bar{\mathbf{C}}} = \mathbf{a}_0\otimes\bar{\mathbf{C}}\,\mathbf{a}_0 + \mathbf{a}_0\,\bar{\mathbf{C}}\otimes\mathbf{a}_0, \quad \frac{\partial^2\bar{I}_5}{\partial\bar{\mathbf{C}}\partial\bar{\mathbf{C}}} = \frac{\partial}{\partial\bar{\mathbf{C}}}(\mathbf{a}_0\otimes\bar{\mathbf{C}}\,\mathbf{a}_0 + \mathbf{a}_0\,\bar{\mathbf{C}}\otimes\mathbf{a}_0),$$

$$\begin{aligned}\bar{\mathbb{C}} = J^{-4/3}\Big(&\bar{\delta}_1\,\mathbf{I}\otimes\mathbf{I} + \bar{\delta}_2\left(\mathbf{I}\otimes\bar{\mathbf{C}} + \bar{\mathbf{C}}\otimes\mathbf{I}\right) + \bar{\delta}_3\bar{\mathbf{C}}\otimes\bar{\mathbf{C}} + \bar{\delta}_4\,\mathbb{S} + \bar{\delta}_5\,(\mathbf{I}\otimes\mathbf{a}_0\otimes\mathbf{a}_0 + \mathbf{a}_0\otimes\mathbf{a}_0\otimes\mathbf{I})\\ &+ \bar{\delta}_6\,(\bar{\mathbf{C}}\otimes\mathbf{a}_0\otimes\mathbf{a}_0 + \mathbf{a}_0\otimes\mathbf{a}_0\otimes\bar{\mathbf{C}}) + \bar{\delta}_7\,(\mathbf{a}_0\otimes\mathbf{a}_0\otimes\mathbf{a}_0\otimes\mathbf{a}_0)\\ &+ \bar{\delta}_8\left(\mathbf{I}\otimes\frac{\partial\bar{I}_5}{\partial\bar{\mathbf{C}}} + \frac{\partial\bar{I}_5}{\partial\bar{\mathbf{C}}}\otimes\mathbf{I}\right) + \bar{\delta}_9\left(\bar{\mathbf{C}}\otimes\frac{\partial\bar{I}_5}{\partial\bar{\mathbf{C}}} + \frac{\partial\bar{I}_5}{\partial\bar{\mathbf{C}}}\otimes\bar{\mathbf{C}}\right) + \bar{\delta}_{10}\left(\frac{\partial\bar{I}_5}{\partial\bar{\mathbf{C}}}\otimes\frac{\partial\bar{I}_5}{\partial\bar{\mathbf{C}}}\right)\\ &+ \bar{\delta}_{11}\left(\mathbf{a}_0\otimes\mathbf{a}_0\otimes\frac{\partial\bar{I}_5}{\partial\bar{\mathbf{C}}} + \frac{\partial\bar{I}_5}{\partial\bar{\mathbf{C}}}\otimes\mathbf{a}_0\otimes\mathbf{a}_0\right) + \bar{\delta}_{12}\frac{\partial^2\bar{I}_5}{\partial\bar{\mathbf{C}}\partial\bar{\mathbf{C}}}\Big)\end{aligned}$$

$$\tilde{\mathbb{P}} = \mathbf{C}^{-1}\odot\mathbf{C}^{-1} - \frac{1}{3}\,\mathbf{C}^{-1}\otimes\mathbf{C}^{-1}$$

$$\mathbb{C}_{\text{iso}} = \mathbb{P}:\bar{\mathbb{C}}:\mathbb{P}^{\top} + \frac{2}{3}\,J^{-2/3}\bar{\mathbf{S}}:\mathbf{C}\,\tilde{\mathbb{P}} - \frac{2}{3}\left(\mathbf{C}^{-1}\otimes\mathbf{S}_{\text{iso}} + \mathbf{S}_{\text{iso}}\otimes\mathbf{C}^{-1}\right)$$

Then, $\mathbb{C} = \mathbb{C}_{\text{vol}} + \mathbb{C}_{\text{iso}}$ can be calculated.

1.3.5 Derivation of the Finite Element Model

To describe muscle contraction, we use a solid mechanics formulation in material description with a reference configuration Ω_0. The quantities of interest are the displacements $\mathbf{u}$, velocities $\mathbf{v} = \dot{\mathbf{u}}$, and stresses in terms of the second Piola-Kirchhoff tensor $\mathbf{S}$:

$$\operatorname{div}_{\mathbf{X}}(\mathbf{v}) = 0, \tag{1.63}$$

$$\operatorname{grad}_{\mathbf{X}}\mathbf{P} + \mathbf{B} = \rho_0 \dot{\mathbf{v}}, \tag{1.64}$$

$$\mathbf{S} = \mathbf{S}^{\top}, \tag{1.65}$$

$$\det \mathbf{F} = 0. \tag{1.66}$$

Here, Eq. (1.63) follows from conservation of mass assuming a constant density ρ_0 for all points $\mathbf{X} \in \Omega_0$. Equation (1.64) is the balance of linear momentum with body forces $\mathbf{B}$ in reference configuration and the first Piola-Kirchhoff stress tensor $\mathbf{P} = \mathbf{F}\,\mathbf{S}$ with the deformation gradient $\mathbf{F}$. The symmetry of the stress tensor $\mathbf{S}$ in Eq. (1.65) follows from conservation of angular momentum. We additionally enforce incompressibility by Eq. (1.66). Dirichlet and Neumann boundary conditions are specified to fix certain displacements and prescribe surface traction forces, respectively. The constitutive relation between stresses and strains is given by a hyperelastic, transversely-isotropic material where an active stress term is added to the passive stress tensor. The formulation is based on **Heidlauf2014a**.

To simulate muscle contraction, we use an incompressible, hyperelastic, transversely-isotropic material where an active stress term is added to the passive stress tensor. The formulation is based on **Heidlauf2014a**. We use a mixed u, v, p-Finite Element formulation with displacements u and velocities v. The hydrostatic pressure p acts as a Lagrange multiplier and allows to fulfill the incompressibility constraint exactly while avoiding locking.

The model equations for the dynamic problem are given by

$$\delta W_{\text{int}}(\mathbf{u}, p) - \delta W_{\text{ext}}(\dot{\mathbf{v}}) = 0 \qquad \forall\, \delta\mathbf{u} \in W_u^h, \tag{1.67}$$

$$\dot{\mathbf{u}} = \mathbf{v}, \tag{1.68}$$

$$\int_{\Omega} \big(J(\mathbf{u}) - 1\big)\, \delta p \, \mathrm{d}V = 0 \qquad \forall\, \delta p \in W_p^h. \tag{1.69}$$

Here, Eq. (1.67) is the principle of virtual work with the internal virtual work δW_{int} and the external virtual work δW_{ext} that contains inertial and gravitational body forces and traction forces. Equation (1.68) connects the displacements and velocities and Eq. (1.69)

is the incompressibility constraint on the determinant J of the deformation gradient.

We discretize the system in space by Taylor-Hood Finite Elements that use quadratic ansatz functions for $\mathbf{u}$ and $\mathbf{v}$ and linear ansatz functions for p on 3D hexaeder elements in Ω_M. We use the implicit Euler method for the time discretization and solve the resulting nonlinear equations in every timestep by a Newton scheme. To speed up the computation, the initial guess of the vector of unknowns in every timestep is linearly extrapolated from the two previous timesteps.

Bibliography

[Car17] **Carniel**, T. A.; **Fancello**, E. A.: *A transversely isotropic coupled hyperelastic model for the mechanical behavior of tendons*, Journal of Biomechanics 54, 2017, pp. 49–57, ISSN: 0021-9290, doi:https://doi.org/10.1016/j.jbiomech.2017.01.042, https://www.sciencedirect.com/science/article/pii/S0021929017300726

[Cis08] **Cisi**, R. R.; **Kohn**, A. F.: *Simulation system of spinal cord motor nuclei and associated nerves and muscles, in a web-based architecture*, Journal of computational neuroscience 25.3, 2008, pp. 520–542

[Cra47] **Crank**, J.; **Nicolson**, P.: *A practical method for numerical evaluation of solutions of partial differential equations of the heat-conduction type*, Mathematical Proceedings of the Cambridge Philosophical Society 43.1, 1947, pp. 50–67, doi:10.1017/S0305004100023197

[Gui03] Godunov-type Schemes, ed. by **Guinot**, V., Amsterdam: Elsevier, 2003, pp. 471–480, isbn:978-0-444-51155-3, doi:https://doi.org/10.1016/B978-044451155-3/50015-3, https://www.sciencedirect.com/science/article/pii/B9780444511553500153

[Hei13] **Heidlauf**, T.; **Röhrle**, O.: *Modeling the chemoelectromechanical behavior of skeletal muscle using the parallel open-source software library opencmiss*, Computational and Mathematical Methods in Medicine 2013, 2013, pp. 1–14, doi:10.1155/2013/517287, http://dx.doi.org/10.1155/2013/517287

[Hei15] **Heidlauf**, T., ed.: *Chemo-electro-mechanical modelling of the neuromuscular system*, Englisch, Text (nur für elektronische Ressourcen), Online publiziert 2016, Stuttgart, 2015, http://nbn-resolving.de/urn:nbn:de:bsz:93-opus-104496

[Hin76] **Hinton**, E.; **Rock**, T.; **Zienkiewicz**, O. C.: *A note on mass lumping and related processes in the finite element method*, Earthquake Engineering & Structural Dynamics 4.3, 1976, pp. 245–249, doi:10.1002/eqe.4290040305

[Hod52a] **Hodgkin**, A. L.; **Huxley**, A. F.: *A quantitative description of membrane current and its application to conduction and excitation in nerve.* The Journal of Physiology 117.4, 1952, pp. 500–544

[Hod52b] **Hodgkin**, A. L.; **Huxley**, A. F.: *Propagation of electrical signals along giant nerve fibres*, Proceedings of the Royal Society of London. Series B, Biological Sciences, 1952, pp. 177–183

[Hol00] **Holzapfel**, A. G.: *Nonlinear solid mechanics*, 2000

[Klo20] **Klotz**, T. et al.: *Modelling the electrical activity of skeletal muscle tissue using a multi-domain approach*, Biomechanics and Modeling in Mechanobiology 19.1, 2020, pp. 335–349, ISSN: 1617-7940, doi:10.1007/s10237-019-01214-5, https://doi.org/10.1007/s10237-019-01214-5

[Mar94] **Marsden**, J. E.; **Hughes**, T. J.: *Mathematical foundations of elasticity*, Courier Corporation, 1994

[Mil06a] **Mileusnic**, M. P.; **Loeb**, G. E.: *Mathematical models of proprioceptors. ii. structure and function of the golgi tendon organ*, Journal of Neurophysiology 96.4, 2006, PMID: 16672300, pp. 1789–1802, doi:10.1152/jn.00869.2005, eprint: https://doi.org/10.1152/jn.00869.2005, https://doi.org/10.1152/jn.00869.2005

[Mil06b] **Mileusnic**, M. P. et al.: *Mathematical models of proprioceptors. i. control and transduction in the muscle spindle*, Journal of Neurophysiology 96.4, 2006, PMID: 16672301, pp. 1772–1788, doi:10.1152/jn.00868.2005, eprint: https://doi.org/10.1152/jn.00868.2005, https://doi.org/10.1152/jn.00868.2005

[Mor15] **Mordhorst**, M.; **Heidlauf**, T.; **Röhrle**, O.: *Predicting electromyographic signals under realistic conditions using a multiscale chemo-electro-mechanical finite element model*, Interface Focus 5.2, 2015, pp. 1–11, doi:10.1098/rsfs.2014.0076, http://dx.doi.org/10.1098/rsfs.2014.0076

[Pes79] **Peskoff**, A.: *Electric potential in three-dimensional electrically syncytial tissues*, Bulletin of mathematical biology 41.2, 1979, pp. 163–181

[Röh12] **Röhrle**, O.; **Davidson**, J. B.; **Pullan**, A. J.: *A physiologically based, multi-scale model of skeletal muscle structure and function*, Frontiers in Physiology 3, 2012

[Sho07] **Shorten**, P. R. et al.: *A mathematical model of fatigue in skeletal muscle force contraction*, Journal of Muscle Research and Cell Motility 28.6, 2007, pp. 293–313, doi:10.1007\%2Fs10974-007-9125-6, http://dx.doi.org/10.1007%5C%2Fs10974-007-9125-6

[Str68] **Strang**, G.: *On the construction and comparison of difference schemes*, SIAM Journal on Numerical Analysis 5.3, 1968, pp. 506–517, doi:10.1137/0705041, eprint: https://doi.org/10.1137/0705041, https://doi.org/10.1137/0705041

[Sus87] **Sussman**, T.; **Bathe**, K.-J.: *A finite element formulation for nonlinear incompressible elastic and inelastic analysis*, Computers & Structures 26.1, 1987, pp. 357–409, ISSN: 0045-7949, doi:https://doi.org/10.1016/0045-7949(87)90265-3, http://www.sciencedirect.com/science/article/pii/0045794987902653

[Tun78] **Tung**, L.: *A bi-domain model for describing ischemic myocardial dc potentials*. PhD thesis, Massachusetts Institute of Technology, 1978

[Zie05] **Zienkiewicz**, O. C.; **Taylor**, R. L.; **Zhu**, J. Z.: *The finite element method: its basis and fundamentals*, Elsevier, 2005

[Zie77] **Zienkiewicz**, O. C.; **Taylor**, R. L.: *The finite element method*, vol. 3, McGraw-hill London, 1977